A&A 614, A149 (2018)
https://doi.org/10.1051/0004-6361/201730562

Astronomy & Astrophysics

Oxygen and zinc abundances in 417 Galactic bulge red giants*

C. R. da Silveira[1], B. Barbuy[1], A. C. S. Friaça[1], V. Hill[2], M. Zoccali[3,4], M. Rafelski[5], O. A. Gonzalez[6], D. Minniti[4,7], A. Renzini[8], and S. Ortolani[9]

[1] Universidade de São Paulo, IAG, Rua do Matão 1226, Cidade Universitária, São Paulo 05508-900, Brazil
e-mail: barbuy@astro.iag.usp.br
[2] Université de Sophia-Antipolis, Observatoire de la Côte d'Azur, CNRS UMR 6202, BP4229, 06304 Nice Cedex 4, France
[3] Pontificia Universidad Católica de Chile, Instituto de Astrofísica, Casilla 306, Santiago 22, Chile
[4] Millenium Institute of Astrophysics, Av. Vicuña Mackenna 4860, Macul, Santiago, Chile
[5] Space Telescope Science Institute, 3700 San Martin Drive, Baltimore, MD 21218, USA
[6] Institute for Astronomy, University of Edinburgh, Royal Observatory, Blackford Hill, Edinburgh EH9 3HJ, UK
[7] Departamento de Ciencias Físicas, Universidad Andres Bello, República 220, Santiago, Chile
[8] Osservatorio Astronomico di Padova, Vicolo dell'Osservatorio 5, 35122 Padova, Italy
[9] Università di Padova, Dipartimento di Astronomia, Vicolo dell'Osservatorio 2, 35122 Padova, Italy

Received 5 February 2017 / Accepted 21 February 2018

ABSTRACT

Context. Oxygen and zinc in the Galactic bulge are key elements for the understanding of the bulge chemical evolution. Oxygen-to-iron abundance ratios provide a most robust indicator of the star formation rate and chemical evolution of the bulge. Zinc is enhanced in metal-poor stars, behaving as an α-element, and its production may require nucleosynthesis in hypernovae. Most of the neutral gas at high redshift is in damped Lyman-alpha systems (DLAs), where Zn is also observed to behave as an α-element.
Aims. The aim of this work is the derivation of the α-element oxygen, together with nitrogen, and the iron-peak element zinc abundances in 417 bulge giants, from moderate resolution ($R \sim 22\,000$) FLAMES-GIRAFFE spectra. For stars in common with a set of UVES spectra with higher resolution ($R \sim 45\,000$), the data are intercompared. The results are compared with literature data and chemodynamical models.
Methods. We studied the spectra obtained for a large sample of red giant stars, chosen to be one magnitude above the horizontal branch, using FLAMES-GIRAFFE on the Very Large Telescope. We computed the O abundances using the forbidden [OI] 6300.3 Å and Zn abundances using the Zn I 6362.34 Å lines. Stellar parameters for these stars were established in a previous work from our group.
Results. We present oxygen abundances for 358 stars, nitrogen abundances for 403 stars and zinc abundances were derived for 333 stars. Having oxygen abundances for this large sample adds information in particular at the moderate metallicities of $-1.6 < [Fe/H] < -0.8$. Zn behaves as an α-element, very similarly to O, Si, and Ca. It shows the same trend as a function of metallicity as the α-elements, i.e., a turnover around $[Fe/H] \sim -0.6$, and then decreasing with increasing metallicity. The results are compared with chemodynamical evolution models of O and Zn enrichment for a classical bulge. DLAs also show an enhanced zinc-to-iron ratio, suggesting they may be enriched by hypernovae.

Key words. Galaxy: bulge – Galaxy: abundances – stars: abundances

1. Introduction

Oxygen and zinc are key elements for the understanding of the star formation rate and chemical enrichment of the Galactic bulge. Oxygen is the prime and most robust probe for testing the timescale of bulge formation, because it has no contribution from SNIa, and because the prescriptions from different authors (e.g. Woosley & Weaver 1995, hereafter WW95; Kobayashi et al. 2006) produce the same behaviour. Woosley et al. (2002) describe the nucleosynthesis production of the different elements. In all cases oxygen is produced in hydrostatic phases of massive star evolution.

Oxygen abundances in bulge field stars have been derived in several studies, among which the most recent are Alves-Brito et al. (2010); Bensby et al. (2013); Friaça & Barbuy (2017); Johnson et al. (2014); Jönsson et al. (2017); Meléndez et al. (2008); Rich et al. (2012); Ryde et al. (2010); Schultheis et al. (2017), and Siqueira-Mello et al. (2016). A review on abundances in the Galactic bulge is given in McWilliam (2016). A more general review on the MW bulge is presented in Barbuy et al. (2018).

Based on the observed [O/Fe] vs. [Fe/H] behaviour, as compared with their chemodynamical models, Cavichia et al. (2014), and Friaça & Barbuy (2017, hereafter FB17), derived a specific star formation rate of bulge formation and chemical enrichment of $\nu_{SF} \approx 0.5$ Gyr^{-1} or a timescale of bulge formation of 2 Gyr. The specific star formation is defined as $\nu_{SF} = 1/M(M_\odot)\mathrm{d}M(M_\odot)/\mathrm{d}t$, which is the ratio of the SFR over the gas mass in $M_\odot$ available for star formation. A best value can be estimated from the reproduction of the observed turnover in

* Observations collected at the European Southern Observatory, Paranal, Chile (ESO programmes 71.B-0617A, 73.B0074A); Table B.1 is only available in electronic form at the CDS via anonymous ftp to http://cdsarc.u-strasbg.fr/ (130.79.128.5) or via http://cdsarc.u-strasbg.fr/viz-bin/qcat?J/A+A/vol/page.

[O/Fe] vs. [Fe/H] by the models, that occur when SNIa start to give a contribution in Fe.

Zinc is key to probe the contribution of hypernovae at the lower metallicities during the bulge chemical enrichment process. The high [Zn/Fe] ratios in bulge metal-poor stars can at present only be explained by enrichment from hypernovae (Kobayashi et al. 2006; Nomoto et al. 2013) as discussed in Barbuy et al. (2015). Zinc enhancements in metal-poor stars were derived in the literature also in halo stars by Cayrel et al. (2004); Nissen & Schuster (2011), in the thick disk by Bensby et al. (2014); Reddy et al. (2006); Mishenina et al. (2011), and in metal-poor bulge stars by Bensby et al. (2013, 2017), and Barbuy et al. (2015).

Zinc is also useful for comparisons with data from damped Lyman-alpha systems (DLAs). DLAs are neutral hydrogen gas systems observed in absorption to background quasars, with minimum hydrogen column densities of 2×10^{20} cm^{-2}. DLAs dominate the neutral gas content at high redshift, and the metallicity in DLAs is observed to decrease with increasing redshift (Pettini et al. 1999; Rafelski et al. 2012, 2014), similar to the decrease of metallicity with age of stars in our Galaxy. Moreover, due to the neutrality of the gas, the metallicity of the gas can be measured quite precisely without ionization corrections, making them a premier site to measure abundances at high redshift. Additionally, DLAs have been found to be α-enhanced and show enhanced [Zn/Fe] ratios (Rafelski et al. 2012).

We have previously studied the oxygen and zinc abundances in the Galactic bulge based on high resolution FLAMES-UVES spectra of 56 bulge giants (Zoccali et al. 2006; Lecureur et al. 2007; Barbuy et al. 2015; FB17). In the present work we derive O and Zn abundances for 417 red giants observed with FLAMES-GIRAFFE, within the same observational programmes as the FLAMES-UVES data, at the Very Large Telescope. The stars were observed in two fields, selected among the four fields observed by Zoccali et al. (2008): Baade's Window (BW) (l = 1.14°, b = −4.2°), and a field at b = −6° (l = 0.2°, b = −6°). These stars had already been analysed by Zoccali et al. (2008), and Gonzalez et al. (2011) derived abundances of the α-elements Mg, Si, Ca, and Ti for the sample.

The sample covers a range in metallicity [Fe/H] that allows us to investigate the bulge chemical evolution history in connection to other Galactic components. It includes 65 stars with [Fe/H] ≤ −0.5, and 14 with [Fe/H] ≤ −1.0, thus covering the required range, to help impose fundamental constraints on chemical enrichment models from oxygen and zinc abundances. This is so because the bulk of the bulge stars cover the metallicity range of ∼−1.3 < [Fe/H] < ∼+0.5 (Hill et al. 2011; Ness et al. 2013; Rojas-Arriagada et al. 2017; Zoccali et al. 2017), so that stars with metallicities in the range of −1.3 < [Fe/H] < −0.8 are important to understand the metal-poor end of the bulge chemical enrichment. A metal-poor end at these relatively high metallicities can be explained by the fast chemical enrichment that takes place in the bulge, rapidly reaching the metallicity of [Fe/H] ∼ −1.0 (e.g. Cescutti et al. 2008, and in prep.; Wise et al. 2012). In other words, the equivalent of [Fe/H] ∼ −3.0 in the halo, is [Fe/H] ∼ −1.0 in the bulge. It can also help to better constrain the interfaces between the old bulge with the inner halo, and the thick disk. Hawkins et al. (2015) suggested that moderately metal-poor stars in the bulge could define the interface of Galactic disk and inner halo, by studying stars within −1.20 < [Fe/H] < −0.55. The connection between thin and thick disks has also been studied by Mikolaitis et al. (2014).

In the present paper we have adopted the chemodynamical evolution models for an old classical bulge described in Barbuy et al. (2015) and FB17, with some modifications. In Sect. 2 the observations are summarized. In Sect. 2 the basic stellar parameters are reported, and the abundance derivation of O and Zn is described. In Sect. 2 results and discussion are presented, including comparison with literature and chemodynamical evolution models. In Sect. 6 O-poor and N-rich field stars are selected. A summary is given in Sect. 6.

Table 1. Fields observed: coordinates, distance to Galactic centre, reddening as adopted in Zoccali et al. (2008), number of stars observed, and typical signal-to-noise ratios.

Field	l (°)	b (°)	R_{GC} (pc)	E(B-V)	N_{stars}	S/N/pixel @620 nm
Baade's window	1.°14	−4.°18	604	0.55	204	40–60
b = −6°	0.°21	−6.°02	850	0.48	213	60–90

2. Observations

The present data were obtained using the FLAMES-GIRAFFE instrument at the 8.2 m Kueyen of the Very Large Telescope, at the European Southern Observatory (ESO), in Paranal, Chile, as described in Zoccali et al. (2008; ESO Projects 071.B-067, 071.B-0014; PI: A. Renzini). Targets are bulge K giants, with magnitudes ∼1.0 above the red clump, originally in four fields.

In the present work, we have analysed stars from two fields, reported in Table 1, among the four fields studied in Zoccali et al. (2008). These two fields were observed in setups HR13 (612.0–640.5 nm), HR14A (630.8–670.1 nm) and HR15 (660.7–696.5 nm), with resolving power respectively of R = 26 400, 18 000, and 21 350. The other two fields, NGC 6553 field at (l,b) = (5.°25, 3.°02) and Blanco field at (l,b) = (0°,12°), observed with setups HR11, HR13, and HR15, were reanalysed by Johnson et al. (2014), chosen by them because the HR11 setup contains copper lines. They derived abundances of the light elements Na, Al, α-elements O, Mg, Si and Ca, and the Fe-peak elements Cr, Fe, Co, Ni, and Cu, for 156 red giants in those fields.

Given that the same stars observed with FLAMES-UVES were also observed with FLAMES-GIRAFFE, the oxygen and zinc were derived also from the GIRAFFE spectra. The fits to both UVES and GIRAFFE spectra are shown in Appendix A for the stars in common between the two.

The sample consists of red giant branch (RGB) stars, chosen to be ∼1.0 magnitude above the horizontal branch, consequently this sample does not include red clump (RC) stars, as is the case of more recent surveys (e.g. Ness et al. 2013; Rojas-Arriagada et al. 2017; Zoccali et al. 2017). Such a selection was intended to exclude brighter RGB stars in order to avoid spectra with strong TiO lines. The V, I and astrometric positions are from the OGLE catalogue (Udalski et al. 2002), a pre-FLAMES catalogue (Momany et al. 2001), and 2MASS (Carpenter, 2001), as described in Zoccali et al. (2008). The stars' names follow the observational strategy: the targets were divided into two samples, bright and faint, in order to optimize exposure time. When a sample was being observed with GIRAFFE, the other one was observed with UVES, and then the two were swapped. The total exposure time varied from about 1 h to almost 5 h, depending on the setup and on the star luminosity, in order to ensure that the final S/N per pixel, of each co-added spectrum to reach ∼60 (see mean S/N per field in Table 1). Therefore the identifications are Baade's window bright (BWb) and faint (BWf), and the same for the −6 degree field with bright

stars identified by B6b, and faint ones by B6f. These identifications for the UVES stars are inverted for the GIRAFFE identifications, that is, a BWb or B6b star in UVES will be a BWf or B6f in GIRAFFE, with numbers at random, corresponding to a random allocation of fibres for the observations with GIRAFFE.

3. Abundance analysis

Elemental abundances were obtained through line-by-line spectrum synthesis calculations, carried out using the code described in Barbuy et al. (2003) and Coelho et al. (2005). The main molecular lines present in the region, namely the CN $B^2\Sigma - X^2\Sigma$ blue system, CN $A^2\Pi - X^2\Sigma$ red system, C_2 Swan $A^3\Pi - X^3\Pi$, MgH $A^3\Pi - X^3\Sigma^+$, and TiO $A^3\Phi - X^3\Delta$ γ and $B^3\Pi - X^3\Delta$ γ' systems were taken into account. The atmospheric models were obtained by interpolation in the grid of spherical and mildly CN-cycled ([C/Fe] = 0.13, [N/Fe] = +0.31) MARCS models by Gustafsson et al. (2008). These models consider [α/Fe] = +0.20. These models were chosen as these C and N abundances are compatible with the C, N values in normal red giants, and have suitable α-element enhancements.

We adopted the stellar parameters established by our group, given in Zoccali et al. (2006, 2008), and reported in Table B.1. A brief description of the methods follows:

- Photometric colours [V,I] were used together with colour-temperature calibrations by Ramírez & Meléndez (2005). Another useful indicator was also used: the intensity of TiO bands. Given that RGB stars were chosen, intentionally not very bright, in order to avoid too strong TiO bands, it was possible to define a TiO band index, measuring its strength at 6190–6250 Å, for stars with $T_{\rm eff} < 4500$ K (see Zoccali et al. 2008 for further details). Effective temperatures were then checked by imposing excitation equilibrium for FeI and FeII lines of different excitation potential, using about 60 FeI lines, selected to be suitable for metallicities down to [Fe/H] ~ -0.8, and another line list for more metal-poor stars.

  Since the final temperatures are spectroscopic, the reddening $E(B-V)$ and photometric temperatures were used only as initial guesses. The values of reddening reported in Table 1 are from Zoccali et al. (2006, 2008), and are compatible with the minimum values given in Schlafly & Finkbeiner (2011) in fields of 2°.[1]
- Photometric gravities of the sample stars were obtained adopting a classical relation, where the bolometric corrections were obtained using relations by Alonso et al. (1999).
- Microturbulent velocities $v_{\rm t}$ were determined by imposing a constant [Fe/H] derived from FeI lines of different expected equivalent widths.
- Finally, the metallicities for the sample stars were derived using a set of equivalent widths of Fe I lines.

These stellar parameters were also adopted by Gonzalez et al. (2011), for the derivation of α-element abundances. For stars in common with the UVES data, the stellar parameters derived by Zoccali et al. (2006) from FLAMES-UVES data were used.

In Zoccali et al. (2006) and Lecureur et al. (2007), the oxygen abundance for the 56 giants observed with FLAMES-UVES were derived. In Barbuy et al. (2015) these values were revisited, with the unique aim of obtaining reliable CN strengths. In FB17 the oxygen abundances in stars of this sample, observed with both UVES and GIRAFFE spectrographs, were further revised by taking into account in more detail the abundances of carbon based on the C_2(0,1) bandhead at 5635.2 Å and the C I 5380.3 Å line. These derivations replace the previous values by Zoccali et al. (2006), and Lecureur et al. (2007). A mean [C/Fe] = -0.07 ± 0.09 was found for the UVES sample. Recently, Jönsson et al. (2017) and Schultheis et al. (2017) reanalysed a fraction of the FLAMES-UVES sample.

3.1. Zinc

In Barbuy et al. (2015), we derived zinc abundances for 56 red giants observed with the FLAMES-UVES spectrograph. The Zn I 4810.53 and 6362.34 Å lines were used to derive the zinc abundances. The sample in the present work contains 23 stars observed with UVES. We revised the Zn abundances from the Zn I 4810.53 Å line observed with UVES for stars in common with the present sample. The abundances from Barbuy et al. (2015) are reported in Table 2. In a few cases a corrected value is indicated in bold face.

In the present work, the FLAMES-GIRAFFE spectra contain the Zn I 6362.34 Å line alone. As mentioned above, in Appendix A the fits to this line with both UVES and GIRAFFE spectra are shown, for the stars common to the two samples. Literature and adopted oscillator strengths were reported, together with blending lines in Table 1 of Barbuy et al. (2015). The effect of a continuum lowering in the range ~6360.8–6363.1 Å, due to the Ca I 6361.940 autoionization line was taken into account. The continuum in the range 6361–6362 Å was the prime reference for fitting the Zn line, where the effects of the Ca I autoionization line put this region and the Zn I line at the same continuum level. The *FWHM* of lines was fitted for each star for a region around the Zn I line.

The Zn I 6362.339 Å line is sometimes blended with CN lines, as extensively discussed in Barbuy et al. (2015). For this reason, it is necessary to have a suitable derivation of C, N, and O abundances. In the present work we have derived Zn abundances for 333 stars among the 417 sample ones, where the line was well defined.

3.2. Carbon, nitrogen, and oxygen abundances

The derivation of C, N, and O abundances proceeded as described below.

Carbon: since the present spectra have neither the Swan C_2 (0,1) $A^3\Pi - X^3\Pi$ bandhead at 5635 Å, nor the C I 5380.3 Å line, and in the absence of a reliable C abundance indicator, we adopted a value of [C/Fe] = −0.2 for all stars, a deficiency expected in red giants (e.g. Smiljanic et al. 2009), compatible with the mean [C/Fe] = −0.07 found for the UVES sample, see FB17, their Table A.1. For stars that are also observed with UVES, as well as with Zoccali et al. (2006); Barbuy et al. (2015), and FB17, the UVES results are preferred. The effect of C abundance in the O abundance is illustrated in Barbuy (1988, their Fig. 2). The N abundance, as derived from a CN bandhead depends on the C abundance adopted. Despite an uncertainty on the N abundance due to this assumption, we remind the reader that the main aim here is to be able to reproduce the CN line intensities, given the blend with CN lines on the right wing of the Zn I 6362.339 Å line.

Nitrogen: we used the red CN (5,1) $A^2\Pi - X^2\Sigma$ bandhead at 6332.18 Å, to derive N abundances, adopting the laboratory line list by Davis & Phillips (1963). Nitrogen abundances are important for the dissociative equilibrium between C, N, and O (e.g.

[1] http://irsa.ipac.caltech.edu/applications/DUST/.

Tsuji 1973; Irwin 1988). In red giants N abundances are more informative on the CN-cycle than on chemical evolution. This is due to the transformation of C into N due to the CNO-cycle that takes place along the ascent of the giant branch. Added to the expected mixing process, there is an observed extra-mixing (see e.g. Smiljanic et al. 2009). Therefore the enhanced N abundances observed are due to stellar evolution processes, and do not reflect necessarily the N abundance of the gas from which the star formed. The very few cases of very high nitrogen abundances, combined with low oxygen abundances, are discussed in Sect. 6.

Oxygen: the forbidden oxygen [OI]6300.311 Å line was used to derive O abundances, adopting log gf = −9.716, and taking into account the blends with Ni I lines at 6300.300 and 6300.350 Å, where we adopted Ni abundances varying in lockstep with Fe, as expected (e.g. Bensby et al. 2014, 2017). A solar abundance of A(O) = 8.76 is adopted (Steffen et al. 2015).

In conclusion, the abundances of N, O and Zn were derived iteratively in this order. The CN line intensity that appears as an asymmetry on the right wing of the Zn I 6362 Å line, is also used to check the N and O abundances.

Table B.1 gives the atmospheric parameters adopted from Zoccali et al. (2008), and the resulting N, O, and Zn abundances for 417 stars in Baade's window and the −6 degree fields. In Table 2 are presented the abundances derived for N, O, and Zn for the 23 sample stars having FLAMES-UVES spectra. The Zn abundances from the ZnI 4810 Å line were revised, and slightly modified in a few cases (indicated in bold face). For deriving the present N, O, and Zn abundances for these stars, we adopted the parameters from the UVES analysis (Zoccali et al. 2006; Lecureur et al. 2007). As explained above (Sect. 3), the C, N, and O abundances reported first in Zoccali et al. (2006) and Lecureur et al. (2007), were partially revised in Barbuy et al. (2015), and the revision was further completed by FB17, and these latter are the values adopted here.

In Table 3 we report the stellar parameters and N, O, and Zn abundances for the 23 stars from both UVES and GIRAFFE data. In Fig. 1 we compare the abundances of O, N, and Zn derived from the GIRAFFE data with those derived from the UVES spectra. The oxygen abundances are in very good agreement. Nitrogen abundances appear somewhat higher in GIRAFFE spectra with respect to those in UVES. For N we could not refit C, since we have no atomic or molecular line for this element, and this may be the source of the discrepancy. Zinc tends to be lower in GIRAFFE spectra than in the UVES ones; in Fig. 1 the difference is larger for the UVES values given for the mean of abundances derived from the two lines Zn I 4810.5 and 6362.3 Å, and less discrepant when comparing results for the same line as in the GIRAFFE spectra.

3.3. Errors

For stars in common with UVES, we adopted the same uncertainties given in Barbuy et al. (2013), amounting to $T_{\rm eff}$ ± 150 K for effective temperature, log g ± 0.20 for surface gravity, [Fe/H] ± 0.10 in metallicity, and $v_{\rm t}$ ± 0.10 km s^{-1} for microturbulent velocity. For the stars that have only GIRAFFE spectra we adopted higher uncertainties, due to having a lower resolution in the measurements of Fe I and Fe II lines, of ±200 K for $T_{\rm eff}$, ±0.40 for log g, ±0.10 in [Fe/H] and ±0.30 km s^{-1} for microturbulent velocity.

The errors in [O/Fe] and [Zn/Fe] are computed by using model atmospheres with parameters changed by these uncertainties, applied to the representative stars: the cooler star BW-b6, and the hotter star B6-b3. Both of these were also analysed by Jönsson et al. (2017), as shown in Table 5.

These uncertainties are given in Table 4. Since the stellar parameters are covariant, the sum of these errors is an upper limit. On the other hand, a continuum location uncertainty introduces a further uncertainty in [O/Fe] ∼ ±0.05 and [Zn/Fe] ∼ ±0.05.

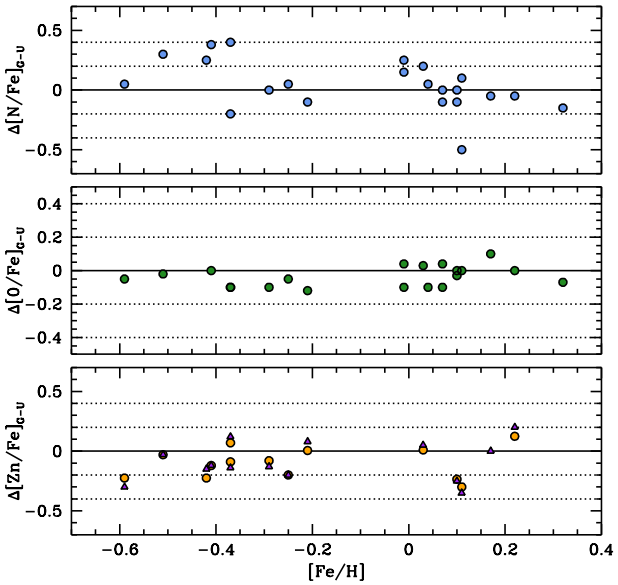

Fig. 1. Comparison between GIRAFFE and UVES abundances for O, N, and Zn for the stars common to the two sets of spectra (Table 3). For Zn: orange full circles consider the mean of two lines in the UVES results, and violet full triangles compare results for the same line.

4. Results

Table B.1 reports the stellar parameters by Zoccali et al. (2008) for the GIRAFFE sample. For stars for which we have both UVES and GIRAFFE spectra, the two sets of parameters and results are reported in Table B.1, with the UVES ones first, marked with a star (*), and the GIRAFFE ones just below. In this Table are given the OGLE, GIRAFFE and UVES names, stellar parameters, the derived N, O and Zn abundances, and the α-elements Mg, Si, Ca, and Ti analysed by Gonzalez et al. (2011).

4.1. Oxygen abundances

In FB17 we discussed the available previous work on bulge samples with reported derivations of oxygen abundances. These were the bulge dwarfs by Bensby et al. (2013), the red giant stars from Alves-Brito et al. (2010) that were carried out in the optical for the same stars as in Meléndez et al. (2008); Cunha & Smith (2006); Ryde et al. (2010); Rich et al. (2012); Johnson et al. (2014); Rich and Origlia (2005) and Fulbright et al. (2007).

We now compare the present oxygen abundances for the GIRAFFE sample together with those from the UVES sample, given in FB17, compared with: (a) the reanalysis of stellar parameters carried out by Jönsson et al. (2017) for 23 stars of the same UVES data, for which they derived oxygen abundances, except for one of them (B3-f1) that FB17 did not include in their study; (b) Ryde et al. (2010) where five stars of our UVES sample were included, plus another six stars; (c) recent results by Schultheis et al. (2017), where comparisons with a fraction of the present

Table 2. Sample of stars observed with both FLAMES-UVES and FLAMES-GIRAFFE.

GIRAFFE	UVES	[Fe/H]	[N/Fe]	[O/Fe]	[Zn/Fe] (ZnI 4810 Å)	[Zn/Fe] (ZnI 6362 Å)	<[Zn/Fe]>
bwb007	BW-f1	+0.32	+0.45	−0.18	−0.35	−0.30	−0.30
bwb040	BW-f5	−0.59	+0.40	+0.25	**+0.30**	+0.00	+0.15
bwb061	BW-f7	+0.11	+0.70	−0.25	−0.20	+0.00	−0.10
bwb087	BW-f4	−1.21	+0.70	+0.30	+0.30	+0.00	+0.15
bwb096	BW-f6	−0.21	+0.40	+0.20	+0.15	+0.00	+0.08
bwf026	BW-b5	+0.17	+0.05	−0.10	−0.30	−0.30	−0.30
bwf067	BW-b2	+0.22	+0.20	−0.10	**−0.30**	+0.00	−0.15
bwf093	BW-b4	+0.07	+0.00	−0.10	**−0.60**	−0.30	−0.45
bwf102	BW-b6	−0.25	+0.65	+0.15	+0.00	+0.00	+0.00
bwf119	BW-b7	+0.10	+0.10	−0.20	**−0.30**	−0.30	−0.30
b6b044	B6-f5	−0.37	+0.00	+0.10	+0.10	+0.00	+0.05
b6b060	B6-f7	−0.42	+0.30	—	−0.15	+0.00	−0.08
b6b095	B6-f2	−0.51	+0.20	+0.20	+0.05	+0.00	+0.03
b6b122	B6-f1	−0.01	+0.20	+0.03	−0.30	−0.60	−0.45
b6b132	B6-f8	+0.04	+0.30	−0.20	−0.60	−0.30	−0.45
b6b134	B6-f3	−0.29	+0.30	+0.15	+0.10	+0.00	+0.05
b6f010	B6-b1	+0.07	+0.50	+0.00	−0.20	−0.30	−0.25
b6f013	B6-b8	+0.03	+0.10	−0.03	**−0.30**	+0.00	−0.15
b6f016	B6-b3	+0.10	+0.50	−0.12	−0.27	−0.60	−0.44
b6f028	B6-b5	−0.37	+0.30	+0.15	**−0.15**	+0.00	−0.08
b6f062	B6-b2	−0.01	+0.35	+0.00	−0.15	—	−0.15
b6f092	B6-b4	−0.41	+0.15	+0.30	+0.00	+0.00	+0.00
b6f095	B6-b6	+0.11	+0.50	−0.10	**−0.30**	−0.30	−0.30

Notes. Metallicities [Fe/H] are from Zoccali et al. (2006), N, O abundances are from Friaça & Barbuy (2017). [Zn/Fe] from Barbuy et al. (2015) for Zn I 4810.54 Å and if revised they are indicated in bold face; [Zn/Fe] for the Zn I 6362.3 Å line in both UVES and GIRAFFE spectra are shown in Appendix A.

stars were given; (d) recent results for microlensed dwarf stars by Bensby et al. (2017).

Figure 3 shows the [O/Fe] vs. [Fe/H] for the present sample (excluding six N-rich, O-poor stars), plotted together with oxygen abundances from UVES data for stars in common, analysed both by FB17, and Jönsson et al. (2017), as well as Ryde et al. (2010); Schultheis et al. (2017), and Bensby et al. (2017). Also included are recent oxygen abundances for metal-poor stars located in outer bulge fields: five stars from García-Pérez et al. (2013), two stars from Howes et al. (2016), and three stars from Lamb et al. (2017).

In Figs. 3 and 4 we overplot the behaviour of oxygen and zinc respectively, in chemodynamical models representing a classical bulge, as described in FB17, and briefly summarized as follows. The evolution of the model was followed up to 13 Gyr, and although the bulge is formed rapidly the star formation goes on, and the stellar mass is built up during at least ≈3 Gyr, allowing for a contribution from type Ia supernovae (SNIa). The best fit model for oxygen, based on previous data, was assumed to have a specific star formation rate of $\nu_{SF} = 0.5$ Gyr^{-1}, following conclusions by FB17, and Cavichia et al. (2014).

Comparison with literature. Part of the present data set has been under study recently by Jönsson et al. (2017) and Schultheis et al. (2017). Given that this may be considered as a reference sample for bulge studies, it is important to compare these different analyses.

In Table 5 we give the stellar parameters rederived by Jönsson et al. (2017), their oxygen abundances given in ϵ(O)[2], and their [O/Fe] = $\epsilon(O)_* - \epsilon(O)_\odot$ − [Fe/H], assuming $\epsilon(O)_\odot = 8.76$ (Steffen et al. 2015). For a comparison with the present work, the stellar parameters from Zoccali et al. (2006) adopted in the present work and in FB17 are reported in the same table, and in the last column the abundance ratio of oxygen-to-iron as rederived by FB17.

We restrict these comparisons to the BW and −6° samples studied in the present work. For three stars (B6-b3, B6-f3, and B6-f8) the effective temperatures differ by $\Delta T_{\rm eff}$(Zoccali+06-Jönsson+17) = −237 K, +364, and +232 K. For three stars the [O/Fe] value is different by more than 0.2 dex, with [O/Fe](Jönsson+17,FB17): BW-f1: +0.45, −0.18; B6-b3: +0.13, −0.12; B6-f8: +0.03, −0.20, and we inspect these stars in particular more closely.

For these three metal-rich stars: BW-f1, B6-b3, and B6-f8, we employed the new stellar parameters from Jönsson et al. (2017), and rederived the C, N, and O abundances in the same way described in FB17, and the results are reported in Table 5. Only for BW-f1 the oxygen abundance differs from that of Jönsson et al., whereas for the other two stars they are similar. Whereas the [O/Fe] values are comparable, it seems to us that both sets of parameters may be hinting at uncertainties: on the one hand, for some cases the gravities may be too high in Jönsson et al. given that we are dealing with stars located one magnitude above the horizontal branch, and on the other, the Zoccali et al. metallicities for some of the metal-rich stars may be too high. In the mean Δ[Fe/H](Zoccali+06-Jönsson+17)

[2] $\epsilon(X) = log(n(X)/n(H)) + 12$, where n = number density of atoms, is a standard notation.

Table 3. Sample of 23 stars observed with both FLAMES-UVES, and FLAMES-GIRAFFE for comparison purposes.

			UVES							GIRAFFE						
OGLE	UVES	GIRAFFE	$T_{\rm eff}$	log g	[Fe/H]	$v_{\rm t}$	[N/Fe]	[O/Fe]	[Zn/Fe]	$T_{\rm eff}$	log g	[Fe/H]	$v_{\rm t}$	[N/Fe]	[O/Fe]	[Zn/Fe]
433669	BW-f1	bwb007	4400	1.80	0.32	1.6	0.45	−0.18	−0.30	4300	1.67	0.32	1.5	0.30	−0.25	−0.40
240260	BW-f5	bwb040	4800	1.90	−0.59	1.3	0.40	0.25	0.00	5150	2.07	−0.59	1.4	0.45	0.20	0.30
357480	BW-f7	bwb061	4400	1.90	0.11	1.7	0.70	−0.25	−0.10	4800	2.06	0.11	1.4	0.20	−0.25	−0.15
537070	BW-f4	bwb087	4800	1.90	−1.21	1.7	0.70	0.30	0.15	5150	2.14	−1.21	1.1	0.54	0.30	—
392918	BW-f6	bwb096	4100	1.70	−0.21	1.5	0.40	0.20	0.08	4600	1.97	−0.21	1.4	0.30	0.08	0.22
82760	BW-b5	bwf026	4000	1.60	0.17	1.2	0.05	−0.10	−0.30	4300	1.87	0.17	1.5	0.00	0.00	—
214192	BW-b2	bwf067	4300	1.90	0.22	1.5	0.20	−0.10	−0.15	4450	1.96	0.22	1.3	0.15	−0.10	−0.20
545277	BW-b4	bwf093	4300	1.40	0.07	1.4	0.00	−0.10	−0.45	4100	1.84	0.07	1.2	−0.10	−0.20	—
392931	BW-b6	bwf102	4200	1.70	−0.25	1.3	0.65	0.15	0.00	4450	1.89	−0.25	1.5	0.70	0.10	0.20
554694	BW-b7	bwf119	4200	1.40	0.10	1.2	0.10	−0.20	−0.30	4300	1.89	0.10	1.2	0.10	−0.20	−0.10
33058c2	B6-f4	b6b044	4500	1.80	−0.37	1.4	0.00	0.10	0.05	4550	1.84	−0.37	1.7	0.40	0.00	0.08
100047c6	B6-f7	b6b060	4300	1.70	−0.42	1.6	0.30	0.25	−0.08	4350	1.72	−0.42	1.5	0.55	0.25	0.15
90337c7	B6-f2	b6b095	4700	1.70	−0.51	1.5	0.20	0.20	0.03	4850	2.02	−0.51	1.5	0.50	0.18	0.08
23017c3	B6-f1	b6b122	4200	1.60	−0.01	1.5	0.20	0.03	−0.45	4250	1.65	−0.01	1.5	0.35	0.07	0.00
11653c3	B6-f8	b6b132	4900	1.80	0.04	1.6	0.30	−0.20	−0.45	4850	1.91	0.04	1.5	0.35	−0.30	−0.50
21259c2	B6-f3	b6b134	4800	1.90	−0.29	1.3	0.30	0.15	0.05	5000	2.02	−0.29	1.5	0.30	0.05	0.13
29280c3	B6-b1	b6f010	4400	1.80	0.07	1.6	0.50	0.00	−0.25	4350	1.80	0.07	1.5	0.50	0.04	—
108051c7	B6-b8	b6f013	4100	1.60	0.03	1.3	0.10	−0.03	−0.15	4250	1.79	0.03	1.6	0.30	0.00	−0.05
31220c2	B6-b3	b6f016	4700	2.00	0.10	1.6	0.50	−0.12	−0.44	4400	1.81	0.10	1.7	0.40	−0.15	−0.05
31090c2	B6-b5	b6f028	4600	1.90	−0.37	1.8	0.30	0.15	−0.08	4700	1.98	−0.37	1.5	0.10	0.05	0.14
83500c6	B6-b2	b6f062	4200	1.50	−0.01	1.4	0.35	0.00	−0.15	4400	2.00	−0.01	1.4	0.60	−0.10	—
60208c7	B6-b4	b6f092	4400	1.90	−0.41	1.7	0.15	0.30	0.00	4400	1.83	−0.41	1.6	0.53	0.30	0.12
77743c7	B6-b6	b6f095	4600	1.90	0.11	1.8	0.50	−0.10	−0.30	4350	1.78	0.11	1.5	0.60	—	−0.15

Table 4. Uncertainties on the derived [O/Fe] and [Zn/Fe] values for model changes of $\Delta T_{\rm eff}$ = 150, 200 K, $\Delta \log g$ = +0.2, 0.4, $\Delta v_{\rm t}$ = +0.1, 0.2, 0.3 km s^{-1}, for UVES and GIRAFFE data respectively, and corresponding total error, applied to the stellar parameters $T_{\rm eff}$, log g, [Fe/H], $v_{\rm t}$ of stars BW-b6 (4200 K, 1.7, −0.25, 1.3 km s^{-1}), and B6-b3 (4700 K, 2.0, 0.10, 1.6 km s^{-1}).

Star	Element	$\Delta T_{\rm eff}$ (+150 K)	$\Delta \log g$ (+0.2)	Δv_t (+0.1 km s^{-1})	$(\sum x^2)^{1/2}$ (parameters)	Continuum	$(\sum x^2)^{1/2}$ (final)
UVES	[C/Fe](CI)	+0.00	+0.00	+0.00	+0.00	±0.02	0.02
BW-b6	[C/Fe](CH)	+0.00	+0.00	+0.00	+0.00	±0.05	0.05
	[N/Fe]	−0.08	+0.02	+0.00	+0.08	±0.02	0.08
	[O/Fe]	+0.00	+0.02	+0.00	+0.02	±0.05	0.05
	[Zn/Fe]	−0.08	+0.06	+0.00	+0.10	±0.05	0.11
		$\Delta T_{\rm eff}$ (+200 K)	$\Delta \log g$ (+0.4)	Δv_t (+0.2 km s^{-1})	$(\sum x^2)^{1/2}$ (parameters)	Continuum	$(\sum x^2)^{1/2}$ (final)
GIRAFFE	[C/Fe](CI)	+0.00	+0.00	+0.00	+0.00	±0.05	0.05
BW-b6	[C/Fe](CH)	+0.00	+0.00	+0.00	+0.00	±0.05	0.05
	[N/Fe]	−0.10	+0.05	+0.00	+0.11	±0.02	0.07
	[O/Fe]	+0.00	+0.05	+0.00	+0.05	±0.05	0.07
	[Zn/Fe]	−0.10	+0.12	+0.00	+0.16	±0.05	0.17
		$\Delta T_{\rm eff}$ (−150 K)	$\Delta \log g$ (+0.2)	Δv_t (+0.1 km s^{-1})	$(\sum x^2)^{1/2}$ (parameters)	Continuum	$(\sum x^2)^{1/2}$ (final)
UVES	[C/Fe](CI)	+0.08	+0.00	+0.00	+0.08	±0.02	0.08
B6-b3	[C/Fe](CH)	+0.00	+0.00	+0.00	+0.00	±0.05	0.05
	[N/Fe]	+0.08	+0.00	+0.00	+0.08	±0.02	0.08
	[O/Fe]	+0.00	+0.03	+0.00	+0.03	±0.05	0.06
	[Zn/Fe]	−0.05	+0.03	+0.00	+0.06	±0.05	0.08
		$\Delta T_{\rm eff}$ (−200 K)	$\Delta \log g$ (+0.4)	Δv_t (+0.2 km s^{-1})	$(\sum x^2)^{1/2}$ (parameters)	Continuum	$(\sum x^2)^{1/2}$ (final)
GIRAFFE	[C/Fe](CI)	+0.10	+0.00	+0.00	+0.10	±0.05	0.11
B6-b3	[C/Fe](CH)	+0.00	+0.00	+0.00	+0.00	±0.05	0.05
	[N/Fe]	+0.10	+0.00	+0.00	+0.10	±0.02	0.10
	[O/Fe]	+0.00	+0.05	+0.00	+0.05	±0.05	0.07
	[Zn/Fe]	−0.07	+0.06	+0.00	+0.09	±0.05	0.10

Notes. The errors are given such as the difference is the amount needed to recover the correct fit.

~ 0.05dex. Except for a large difference in [O/Fe] for BW-f1, the two sets of results agree rather well, and are well-reproduced by the models.

The uncertainty is made more clear if we compare the parameters of Jönsson et al. (2017), and APOGEE data from Schultheis et al. (2017), with respect to Zoccali et al. (2006, 2008).

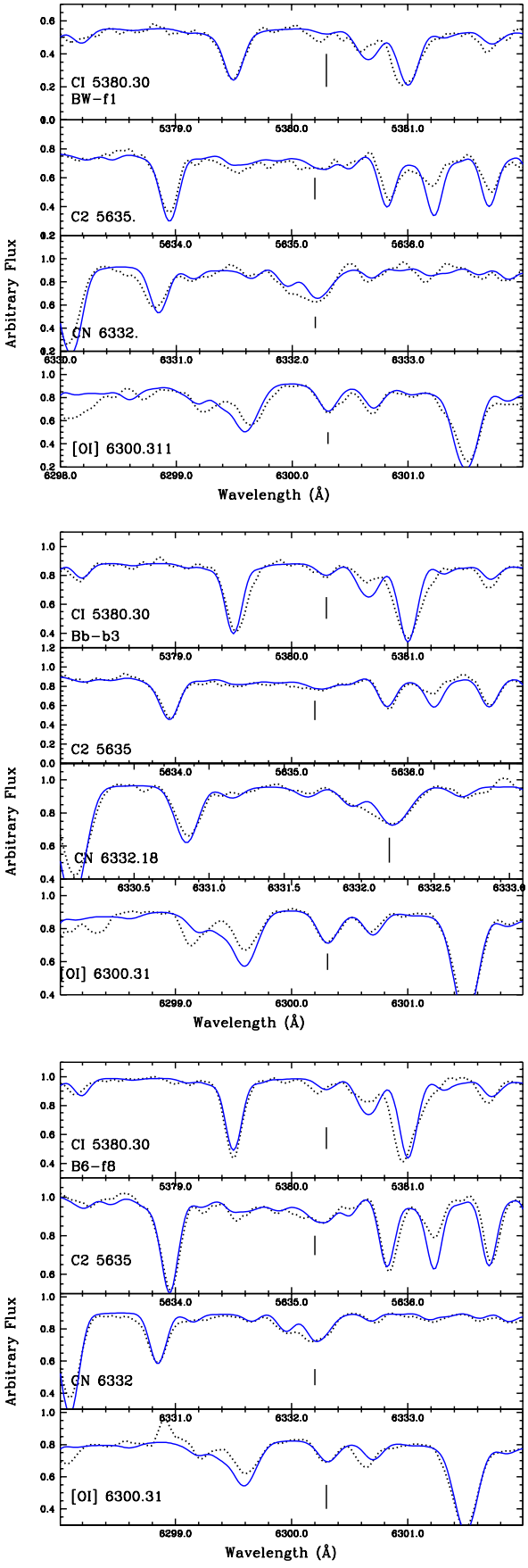

Fig. 2. CNO abundances rederived for stars BW-f1 B6-b3, B6-f8, adopting stellar parameters defined by Jönsson et al. (2017). Symbols: black dotted line: observed spectra; blue solid line: synthetic spectra.

These differences could be taken as the uncertainty expected from different analyses. The comparison of parameters results in the following differences: in effective temperatures $\Delta T_{\rm eff}$ (Jönsson+17-Zoccali+06) = −94 K, and $\Delta T_{\rm eff}$(Schultheis+17-Zoccali+08) = +250 K; and in gravity values $\Delta\log\, g$(Jönsson+17-Zoccali+06) = +0.46 and $\Delta\log\, g$(Schultheis+17-Zoccali+08) = +0.10 (excluding the very discrepant star 2MASS 18042724-3001108). Schultheis et al. (2017) also found Δ[Fe/H] (Schultheis+17-Zoccali+08) = 0.1 dex, and it is different if considering only the metal-poor and metal-rich stars separately where stars with [M/H] < 0 are systematically more metal-poor in Zoccali et al. (2008) with respect to the APOGEE measurements. The differences are larger in effective temperatures with respect to Schultheis et al. and in gravity with respect to Jönsson et al. (2017). The results will become more accurate in the near future, due to the possibility of fixing gravity values with data from the next release of the Gaia Collaboration (2017).

4.2. Zinc abundances

Figure 4 gives [Zn/Fe] vs. [Fe/H] for the sample stars, together with the UVES sample from Barbuy et al. (2015), the recent Zn abundances derived for 90 microlensed bulge dwarf stars by Bensby et al. (2017), and metal-poor stars analysed by Howes (2015); Howes et al. (2014, 2015, 2016) and Casey & Schlaufman (2015). This figure shows that for bulge metal-poor stars with [Fe/H] $\lesssim -1.4$, Zn is enhanced with [Zn/Fe] $\sim +0.4$. This behaviour is in agreement with the same trend of increasing [Zn/Fe] values with decreasing metallicities for thick disk and halo stars as shown in Fig. 7 by Barbuy et al. (2015), where results by Bensby et al. (2014); Ishigaki et al. (2013); Nissen & Schuster (2011); Mishenina et al. (2011); Prochaska et al. (2000); Reddy et al. (2006); Cayrel et al. (2004) were reported.

In Fig. 5, Zn abundances are plotted, compared with the α-element abundances of O, as derived in the present work, and Mg, Si, Ca, and Ti from Gonzalez et al. (2011). The trend shown by Zn appears similar to that of the α-elements, and more closely to oxygen, silicon, and calcium. The low [Zn/Fe] for high metallicity stars is compatible with the oxygen abundances.

Chemodynamical evolution models of zinc were computed for a small classical spheroid, with a baryonic mass of $2\times10^9\ M_\odot$, and a dark halo mass $M_H = 1.3\times10^{10}\ M_\odot$, by Barbuy et al. (2015), FB17. The code allows for inflow and outflow of gas, treated with hydrodynamical equations coupled with chemical evolution.

As discussed in Barbuy et al. (2015), the yields from core-collapse SN II by WW95 underestimate the Zn abundance at low metallicities. Hypernovae, as defined by Nomoto et al. (2006, 2013); Umeda & Nomoto (2002, 2003, 2005), and Kobayashi et al. (2006), reproduce better the enhanced zinc-to-iron abundances in metal-poor stars. There are certain differences with respect to those models in the present work. In Barbuy et al. (2015) the contribution of hypernovae was included for metallicities $Z/Z_\odot \leq 0.0001$, which reproduced well the abundances of DLAs at low metallicities. In the present work, the chemical evolution calculations took into account the core-collapse SN II models of WW95, for metallicities $Z/Z_\odot > 0.01$, and for $Z/Z_\odot < 0.01$ we used a weighted mean of WW95 and the hypernovae yields by Kobayashi et al. (2006), fitting well the data below [Fe/H] $\lesssim -1.6$. There is still an unsolved gap at the moderate metallicities of $-1.6 <$ [Fe/H] < -0.9. There is therefore a mismatch between the models and the data in this metallicity

Table 5. Sample of stars observed with both FLAMES-UVES, and reanalysed by Jönsson et al. (2017).

Star	Jönsson+17						New C, N, O	Zoccali+06				FB17
	$T_{\rm eff}$	log g	[Fe/H]	$v_{\rm t}$	ϵ_*(O)	[O/Fe]	C, N, O	$T_{\rm eff}$	log g	[Fe/H]	$v_{\rm t}$	[O/Fe]
B3-b1	4414	1.35	−0.92	1.41	8.22	+0.38	—	4300	1.7	−0.78	1.5	+0.35
B3-b5	4425	2.70	0.22	1.43	8.87	−0.11	—	4600	2.0	0.11	1.5	−0.30
B3-b7	4303	2.36	0.05	1.58	8.80	−0.01	—	4400	1.9	0.20	1.3	−0.20
B3-b8	4287	1.79	−0.70	1.46	8.47	+0.41	—	4400	1.8	−0.62	1.4	0.30
B3-f1	4485	2.25	−0.18	1.88	8.74	+0.16	—	4500	1.9	0.04	1.6	0.10
B3-f3	4637	2.96	0.21	1.89	8.98	+0.01	—	4400	1.9	0.06	1.7	−0.10
B3-f4	4319	2.60	−0.15	1.50	8.77	+0.16	—	4400	2.1	0.09	1.5	0.10
B3-f8	4436	2.88	0.21	1.54	8.79	−0.18	—	4800	1.9	0.20	1.5	−0.30
BW-b6	4262	1.98	−0.35	1.44	8.60	+0.19	—	4200	1.7	−0.25	1.3	0.15
BW-f1	4359	2.51	0.25	1.93	8.96	+0.45	−0.10, 0.75, 0.00	4400	1.8	0.32	1.6	−0.18
BW-f6	4117	1.43	−0.46	1.69	8.55	+0.25	—	4100	1.7	−0.21	1.5	0.20
BW-f7	4592	2.96	0.53	1.50	9.10	−0.19	—	4400	1.9	0.11	1.7	−0.25
B6-b3	4468	2.48	0.02	1.67	8.91	+0.13	0.15, 0.45, 0.20	4700	2.0	0.10	1.6	−0.12
B6-b4	4215	1.38	−0.65	1.68	8.43	+0.32	—	4400	1.9	−0.41	1.7	0.30
B6-b5	4340	2.02	−0.51	1.34	8.49	+0.24	—	4600	1.9	−0.37	1.8	0.15
B6-b6	4396	2.37	0.16	1.77	8.86	−0.15	—	4600	1.9	0.11	1.8	−0.10
B6-b8	4021	1.90	0.03	1.45	8.68	−0.11	—	4100	1.6	0.03	1.3	−0.03
B6-f1	4149	2.01	0.07	1.65	8.84	+0.01	—	4200	1.6	−0.01	1.5	0.03
B6-f3	4565	2.60	−0.38	1.28	8.63	+0.23	—	4800	1.9	−0.29	1.3	0.15
B6-f8	4470	2.78	0.10	1.30	8.89	+0.03	0.10, 0.25, 0.10	4900	1.8	0.04	1.6	−0.20

Notes. Columns 8–11: stellar parameters from Zoccali et al. (2006); Column 12: [O/Fe] abundances from Friaça & Barbuy (2017).

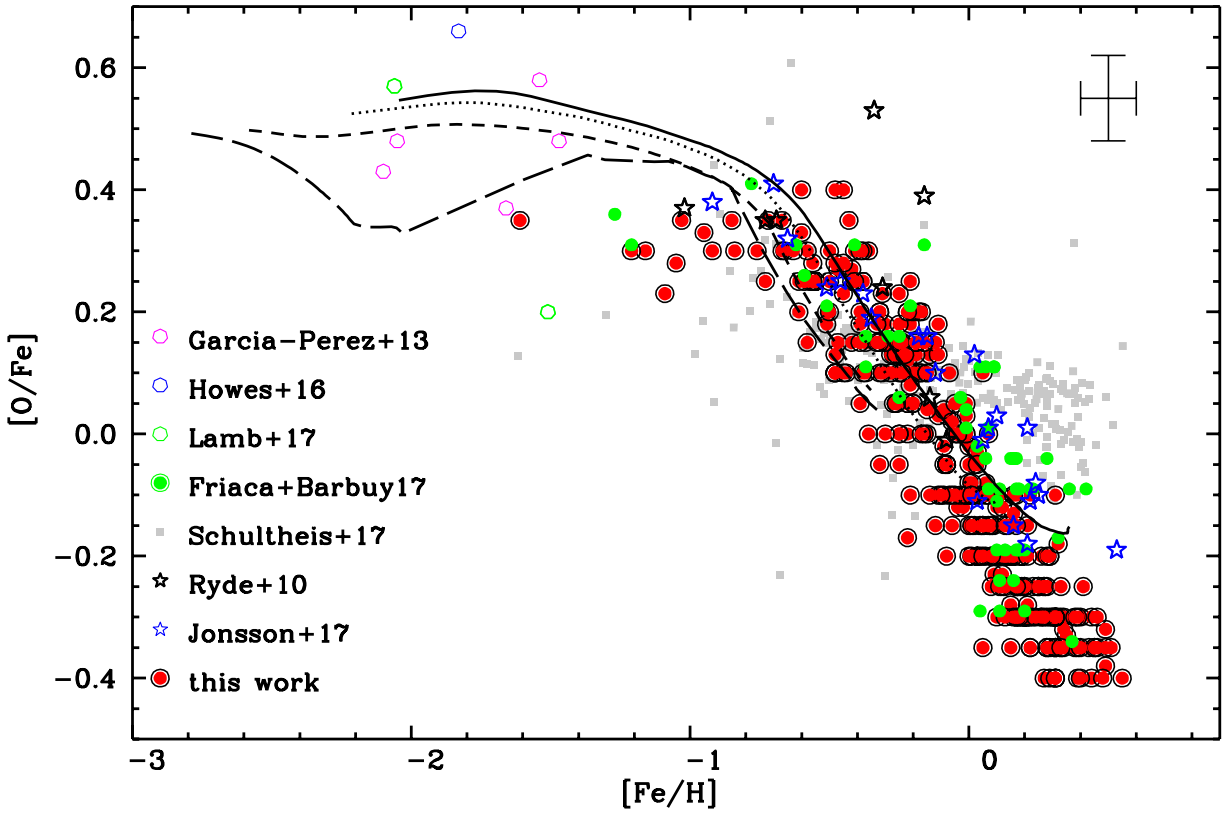

Fig. 3. [O/Fe] vs. [Fe/H] for 351 red giants (excluding N-rich, O-poor ones). Chemodynamical evolution models from FB17 with formation timescale of 2 Gyr, or specific star formation rate of 0.5 Gyr^{-1} are overplotted. Solid lines: 5 < 0.5 kpc; dotted lines: 0.5 < r < 1 kpc; dashed lines: 1 < r < 2 kpc; long-dashed lines: 2 < r < 3 kpc. Symbols: red filled circles: present work; green filled circles: Friaça & Barbuy (2017); blue stars: Jönsson et al. (2017); black stars: Ryde et al. (2010); grey filled squares: Schultheis et al. (2017); magenta open circles: García-Pérez et al. (2013); blue open circles: Howes et al. (2016); green open circles: Lamb et al. (2017). Errors indicated correspond to 0.1dex in both [Fe/H] and [O/Fe]. The model lines correspond to different radii from the Galactic centre: solid lines: r < 0.5 kpc; dotted lines: 0.5 < r < 1 kpc; dashed lines: 1 < r < 2 kpc; long-dashed lines: 2 < r < 3 kpc. A typical error bar is indicated in the right upper corner.

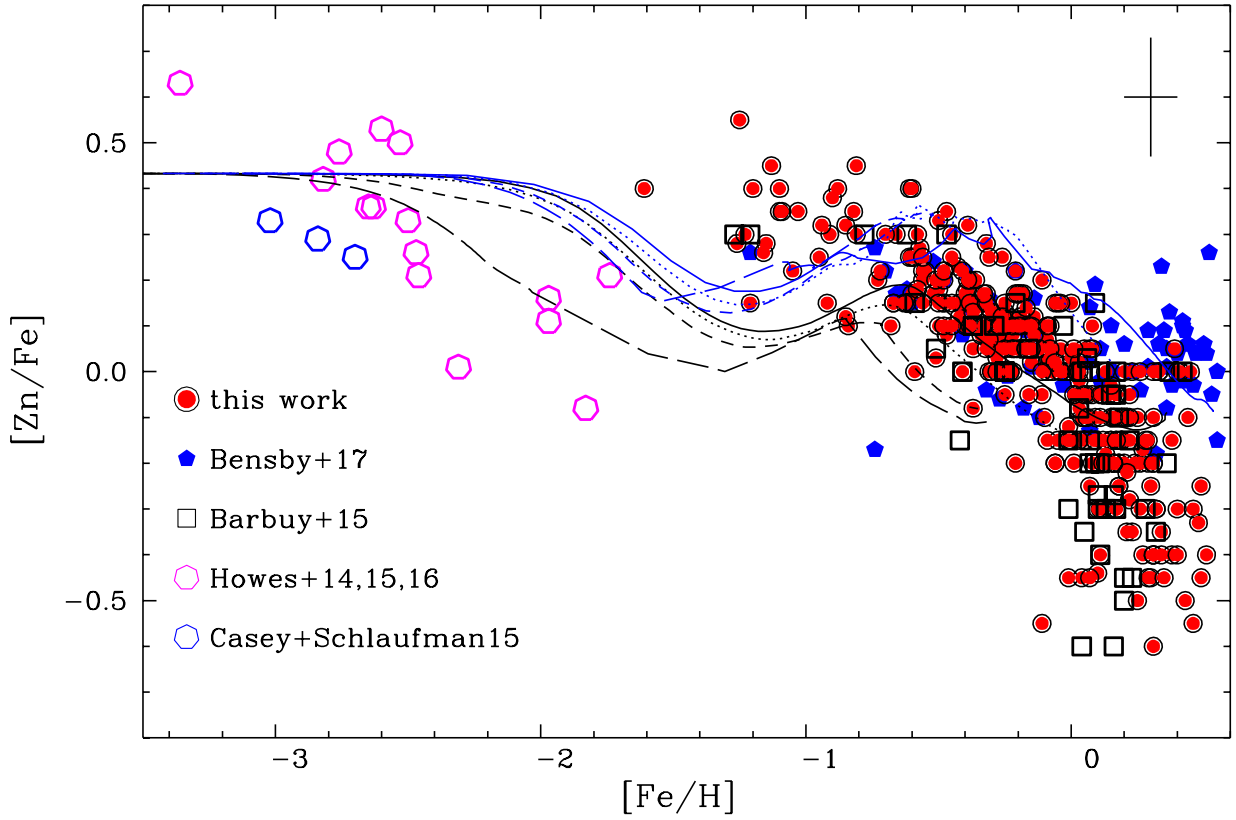

Fig. 4. [Zn/Fe] vs. [Fe/H] for the present sample (333 stars), compared with literature. Symbols: red filled circles: present work; black squares: results for stars in common based on UVES data (Barbuy et al. 2015); blue filled pentagons: Bensby et al. (2017); magenta open heptagons: Howes et al. (2015, 2016); blue open heptagons: Casey & Schlaufman (2015). Chemodynamical evolution models by FB17 with formation timescale of 2 (black lines) and 3 Gyr (blue lines), or specific star formation rate of 0.5, 0.3 Gyr^{-1} are overplotted. The model lines correspond to different radii from the Galactic centre: solid lines: $r < 0.5$ kpc; dotted lines: $0.5 < r < 1$ kpc; dashed lines: $1 < r < 2$ kpc; long-dashed lines: $2 < r < 3$ kpc. A typical error bar is indicated in the right upper corner, corresponding to a mean between the two reference stars (Table 4).

range. It is important to note that chemodynamical models are suitable to indicate the inflexion of the [X/Fe] values due to enrichment of Fe from SNIa.

4.2.1. Comparison with literature

Comparisons with literature Zn abundances of microlensed dwarf bulge stars by Bensby et al. (2013), were discussed in Barbuy et al. (2015). In Fig. 4 we show the updated abundances for microlensed bulge dwarfs by Bensby et al. (2017). There is good agreement between the present results and Barbuy et al. (2015) and those by Bensby et al. at metallicities $-1.4 <$ [Fe/H] < 0.0, whereas the behaviour for metal-rich giants with [Fe/H] > 0.0 are distinct. The microlensed dwarfs show a contant [Zn/Fe], whereas the bulge red giants show a decreasing trend with metallicity, although with a large spread of $-0.6 <$ [Zn/Fe] $< +0.15$.

At the high metallicity end, since there is progressive enrichment in Fe by SNIa, a constant [Zn/Fe] would imply that there is chemical enrichment in both Zn and Fe on similar timescales. Instead, a decrease of [Zn/Fe] would correspond to the enrichment in Fe by SNIa, with no enrichment in Zn by the same SNIa, as happens for the α-elements.

This discrepancy has been addressed by Duffau et al. (2017), who found, at supersolar metallicities, a decreasing [Zn/Fe] for red giants, and constant [Zn/Fe] for dwarfs. Their interpretation is that the dwarfs are old and the red giants are young. This interpretation cannot be applied here, given that at least part of the bulge metal-rich red giant stars should be old, as can be seen in the distribution of ages given in Bensby et al. (2017), see their Figs. 14 and 15).

The derivation of [Zn/Fe] in stars of dwarf galaxies by Skúladóttir et al. (2017; 2018, and references therein) indicated a decreasing [Zn/Fe] with increasing metallicities. This behaviour is in agreement with an Fe enrichment by SNIa, but not with a Zn enrichment.

4.2.2. Comparison with damped Lyman-alpha systems

Comparisons of Zn abundances with data from Akerman et al. (2005); Cooke et al. (2013), and Vladilo et al. (2011) were shown in Barbuy et al. (2015). Using careful dust corrections, Barbuy et al. (2015) concluded that the DLAs fall into the same region of [Zn/Fe] vs. [Fe/H] as thick disk and bulge stars. On the other hand, a comparison of the metallicity of DLAs to thick disk stars in Rafelski et al. (2012) showed that while there is some overlap, the median DLA population is more metal poor than the thick disk stars. While Rafelski et al. (2012) did not apply dust corrections, metallicities were determined using primarily [Si/H] and [S/H], which are less sensitive to dust than [Zn/H]. To investigate this further, we compared the [Zn/Fe] vs. [Fe/H] from our present work to the DLA data presented in Rafelski et al. (2012) in Fig. 6. These data include a compilation of previous DLA systems selected to be unbiased with regard to their metallicities, including those from Akerman et al. (2005) and a subset of Vladilo et al. (2011). We note that the comparison in Fig. 6 must be taken with caution, because there are potential biases with the [Fe/Zn] values that are difficult to control. In the metal

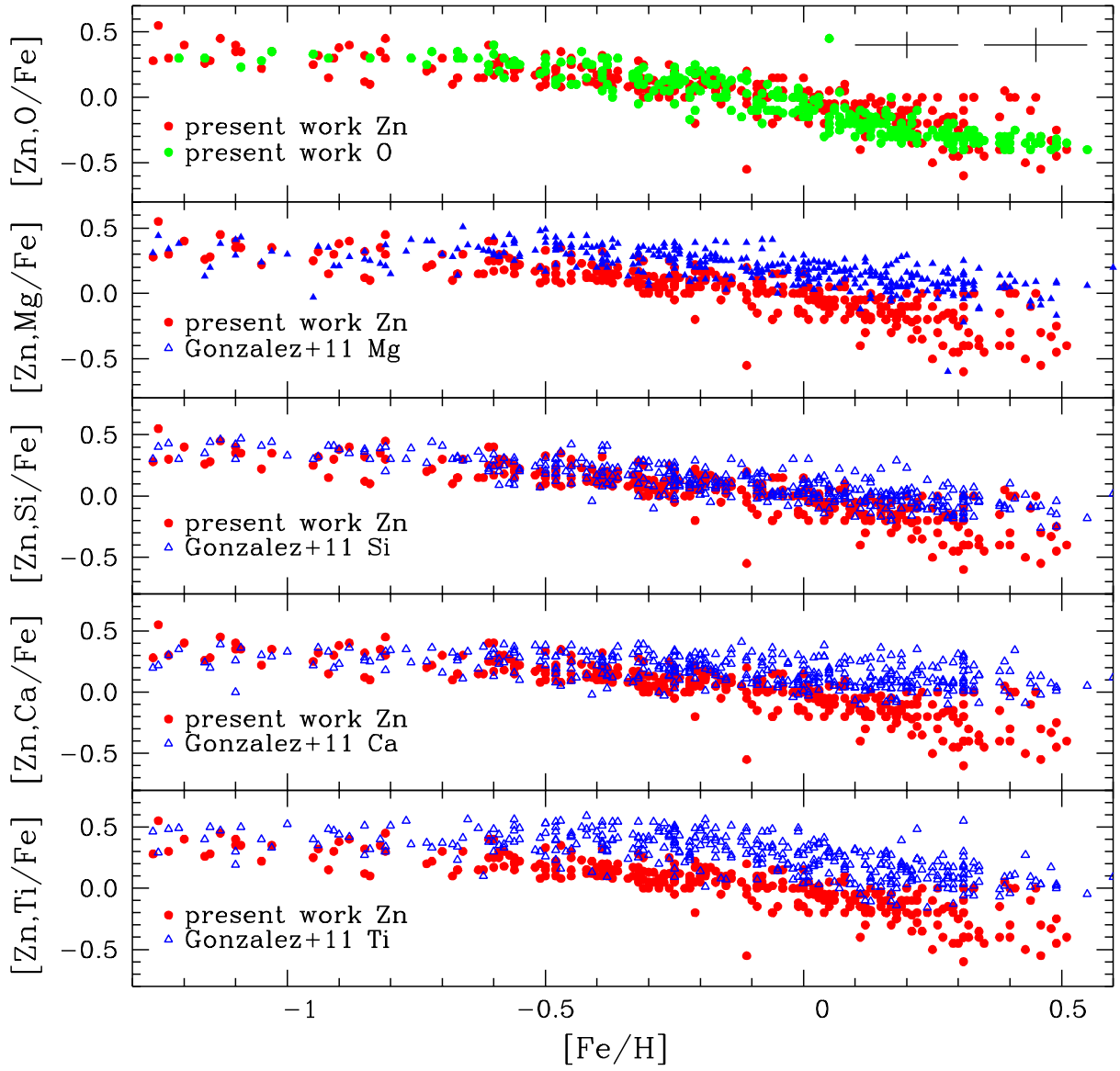

Fig. 5. [O, Mg, Si, Ca,Ti/Fe] vs. [Fe/H] and [Zn/Fe] vs. [Fe/H] for the 417 red giants. Symbols: Red filled circles: O from this work; Green filled circles: Zn from this work; Blue open triangles: Mg, Si, Ca, and Ti from Gonzalez et al. (2011). Typical error bars are indicated for [α/Fe] and [Zn/Fe].

rich regime, Fe is strongly depleted by dust, while on the metal-poor side, the oscillator strengths of Zn result in the absorption lines too weak to be detected in low-metallicity systems. To reduce the biases from dust depletion and undetected Zn absorption lines, we limited our comparison in Fig. 6 to systems with $-2.5 < [\alpha/\mathrm{H}] < -1.0$. In this comparison, no correction for dust is applied.

Figure 6a shows an enhanced zinc-to-iron ratio for the DLA data which is consistent with the present sample, although DLAs typically reside at lower metallicities. We note that Fig. 6 exaggerates the difference in metallicity ([Fe/H]) due to the removal of higher metallicity systems to avoid biases caused by dust depletion of Fe. Other literature data similarly show a spread in [Zn/Fe] (Akerman et al. 2005; Cooke et al. 2013 – see Barbuy et al. 2015), but is also compatible with a [Zn/Fe] enhancement. Cooke et al. (2015) argue instead that [Zn/Fe] in DLAs can be assumed to drop to solar at [Fe/H] ≈ -2.0, based on a compilation of halo stars data by Saito et al. (2009). They assume therefore that Zn tracks Fe for [Fe/H] > -2.0. However, we show in Fig. 6a that both the present sample and the DLAs have elevated [Zn/Fe] at $-2.5 < [\alpha/H] < -1.0$. Moreover, in Rafelski et al. (2012), we find that Zn and S trace each other one-to-one, not consistent with the solar value, but rather consistent with the models in Fenner et al. (2004), suggesting that Zn behaves like an α-element in DLAs, meaning that it is enhanced in metal-poor DLAs. In conclusion, Zn and α-elements show similar behaviour in metal-poor DLAs, and so can be expected to trace one another.

Figure 6a and b show a large scatter in the [Zn/Fe] and [α/Fe] in DLAs, due to varying star formation histories of the galaxies hosting DLAs, and due to variations of dust depletion for different sightlines. There may also be variations due to the complexities in the way Zn is produced. While Fe is produced in SNe Ia, Zn is produced in massive stars (WW95; Umeda & Nomoto 2002). The value of [Zn/Fe] in DLAs therefore likely depends on both the star formation histories of the host galaxies (Fenner et al. 2004) and on possible dust depletion in Fe for any individual sightline. Therefore a complementary investigation

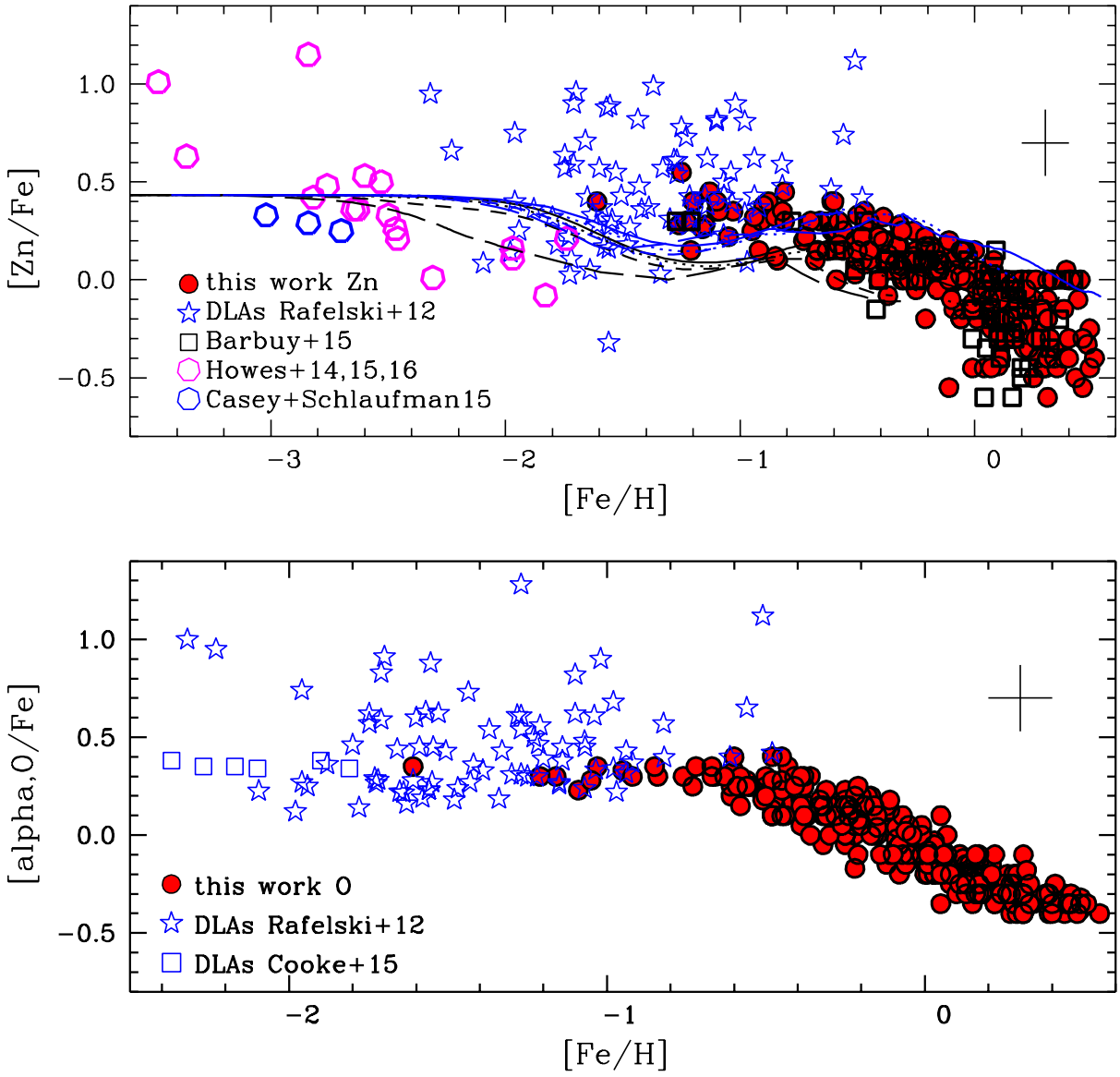

Fig. 6. *Panel a:* [Zn/Fe] vs. [Fe/H]: same as in Fig. 4, including the damped Lyman-alpha systems data by Rafelski et al. (2012). Models from FB17 are overplotted (same details as in Fig. 4); *panel b:* [α/Fe] vs. [Fe/H]: data by Rafelski et al. (2012), [O/Fe] in DLAs by Cooke et al. (2015) and present results for [O/Fe] in the sample stars. The model lines in *panel a:* correspond to the same Galactic bulge radii as in Fig. 4. A typical error bar is indicated in the right upper corner in both panels: for [Zn/Fe] it corresponds to a mean value of the two reference stars given in Table 4. For [α/Fe] the error is of ±0.10 for both the stars and DLAs.

can be accomplished by studies of the α-enhancement [α/Fe] at [α/H] $\lesssim -1.0$.

Figure 6b shows an α-element enhancement of DLAs at [Fe/H] < -1.0 compared with [O/Fe] values for the present sample. In Fig. 6b we also include [O/Fe] values derived for metal-poor DLAs by Cooke et al. (2015). The enhanced [α/Fe] for stellar data with [Fe/H] $< \sim -0.6$, is consistent with the alpha-element enhancement of the DLA data.

5. Oxygen-poor, nitrogen-rich stars

Enhanced nitrogen is expected in red giants due to CN-cycle (Iben 1967), and extra-mixing (e.g. Smiljanic et al. 2009, as reviewed by Karakas & Lattanzio 2014, and references therein). The situation is different for N-rich and O-poor stars, which were first detected in globular clusters (e.g. Sneden et al. 1997). These stars are not only O-poor and N-rich, but also Na-rich, and anomalous also in Mg and Al. In the case of bulge red giants, Schiavon et al. (2017) identified N-rich stars, with a peak in metallicity at [Fe/H] ~ -1.0. They included in this category stars with [N/Fe] $\gtrsim +0.5$, which in their sample of 5140 bulge giants, correspond to 58 of them, therefore in a proportion of 1.1%. Schiavon et al. interpreted these stars as second generation members evaporated from globular clusters. Carretta et al. (2009) have shown that second generation stars have low O, and high N and Na.

For this reason, for the N-rich as defined in Schiavon et al. (2017) with [N/Fe] $\gtrsim +0.5$ stars in our sample, we also measured their Na abundances, using the Na I 6154.23 and 6160.75 Å lines, adopting a hyperfine structure for total values of log gf = −1.56 and −1.26, respectively. The N-rich stars fall in different cases, in terms of N, O: (i) N-rich and O-poor, but for some of them we could not derive [O/Fe] due to blends with telluric lines, and only a N-enhancement is reported; (ii) N-rich and O-normal

Table 6. N-rich and/or O-poor stars.

Star	[Fe/H]	[N/Fe]	[O/Fe]	[Mg/Fe]	[Na/Fe]
N-rich, O-poor stars					
bwb008	−0.80	1.00	0.00	0.15	+0.45
bwb122	−0.81	0.70	−0.05	0.21	+0.25
bwb128	−0.82	0.70	0.00	0.23	+0.15
bwb130	−0.85	0.70	0.10	0.26	+0.15
b6b100	−0.40	0.50	0.00	0.36	+0.00
b6b011	−1.13	1.00	—	0.38	+0.00
b6b016	−0.81	0.70	—	0.37	−0.10
N-rich, O-normal stars					
bwb087	−1.21	0.70	0.30	0.38	+0.20
bwb091	−0.60	0.50	0.40	0.40	−0.15
bwb093	−0.67	0.80	0.30	0.15	−0.30
bwb102	−0.50	0.50	0.20	0.15	−0.05
b6b009	−1.03	0.50	0.35	0.35	−0.30
b6b021	−0.76	0.70	0.30	0.41	+0.00
b6b024	−1.16	0.50	0.30	0.26	−0.20
b6b048	−0.95	0.50	0.33	0.25	−0.30
b6b062	−0.60	0.60	0.33	0.17	−0.05
b6b072	−0.57	0.60	0.25	0.27	+0.10
b6b077	−0.84	0.50	0.30	0.10	−0.30
b6b083	−0.50	0.50	0.30	0.18	+0.00
b6f037	−0.51	0.50	0.18	0.20	+0.30
Very N-rich, high metallicity star					
b6f015	+0.08	1.10	—	—	+0.10

Notes. Na abundances are a mean of abundances from Na I 6154.23 and 6160.75 Å lines.

with [Fe/H] ≤ −0.5; (iii) one star very N-rich [N/Fe] > 1.0 with [Fe/H] = +0.08 ([OI] line is blended with telluric lines in this case). These selected stars are listed in Table 6, where besides the [Na/Fe] value reported, [Mg/Fe] values are also given for an indication of the α-element enrichment in these stars as compared with the oxygen abundances.

If the criterion of [N/Fe] ≥ 0.5 for stars with [Fe/H] ≤ −0.5, is adopted, we find 21 stars, corresponding to about 5% of the sample. If we consider the N-rich ones together with [Na/Fe] > 0.0, then we have 3.5% of them. Finally, if we discard the N-rich but O-normal, keeping only the O-poor ones ([O/Fe] ≲ 0.1), then we have five stars left, corresponding to about 1% of the sample, in agreement with the percentage given by Schiavon et al. (2017). It would be interesting to derive Al for these stars in order to verify a possible Mg-Al anticorrelation also detected in second generation globular cluster stars. The cause of these anomalies is currently under debate in the literature, with the more massive low-Z asymptotic giant branch stars as the likely site for such nucleosynthesis products (Renzini et al. 2015).

6. Summary

We studied oxygen and zinc abundances for 417 field red giants in the Galactic bulge. We were able to derive Zn, O, and N abundances for 333, 358 and 403 of them, respectively. We have identified five stars, corresponding to a 1% of stars that are simultaneously N-rich ([N/Fe] > 0.5), and O-poor ([O/Fe] ≲ 0.1), and this reduces to four stars if the more rigorous criterion of also being Na-rich ([Na/Fe] > 0.0) is applied. According to Schiavon et al. (2017), these characteristics could be attributed to evaporated second generation stars of globular clusters.

The sample contains a number of moderately metal-poor stars (−1.7 < [Fe/H] < −0.5) that define better the behaviour of [O/Fe] and [Zn/Fe] vs. [Fe/H] in this metallicity range. The present chemodynamical evolution modelling of a classical bulge is able to reproduce the behaviour of O and Zn abundances in the Galactic bulge, except for Zn in the range ∼−1.6 ≲ [Fe/H] ≲ −0.8, where the yields from WW95 show a drop. We remind the reader that the models presented here consider yields from WW95 for [Fe/H] > −2.0, and a mean of models by WW95 and Kobayashi et al. (2006) for −4 < [Fe/H] < −2.

The high [Zn/Fe] in very metal-poor stars favours enrichment from hypernovae, as defined by Nomoto et al. (2013 and references therein) acting at these low metallicities. In damped Lyman-alpha systems (DLAs), a high [Zn/Fe] in metal-poor DLAs is also well reproduced by hypernovae yields. In DLAs Zn appears to behave similarly to α elements, and show an enhancement of [α/Fe] similar to the metal poor stars in the present sample. At the metal-rich end, a discrepancy persists between a decreasing [Zn/Fe] with increasing metallicity in the present sample of red giants, and an approximately constant [Zn/Fe] with metallicity for dwarf bulge stars. In conclusion, studies of the Galactic bulge with high-resolution spectroscopy for several hundred stars such as the present study, as well as work based on APOGEE data by Schiavon et al. (2017), and Schultheis et al. (2017), are crucial to better understand the chemical evolution and formation of the Galactic bulge.

Acknowledgements. CRS acknowledges a CAPES/PROEX PhD fellowship. BB and AF acknowledge partial financial support by CNPq, CAPES and FAPESP. MZ and DM acknowledge support by the Ministry of Economy, Development, and Tourism's Millenium Science Initiative through grant IC120009, awarded to The Millenium Institute of Astrophysics, MAS, and from the BASAL Center for Astrophysics and Associated Technologies PFB-06 and FONDECYT Projects 1130196 and 1150345. SO acknowledges the Italian Ministero dell'Università e della Ricerca Scientifica e Tecnologica (MURST), Italy.

References

Akerman, C. J., Ellison, S. L., Pettini, M., & Steidel, C. C. 2005, A&A, 440, 499
Alonso, A., Arribas, S., & Martínez-Roger, C. 1999, A&AS, 140, 261
Alves-Brito, A., Meléndez, J., Asplund, M., et al. 2010, A&A, 513, A35
Asplund, M., Grevesse, N., Sauval, A. J., & Scott, P. 2009, ARA&A, 47, 481
Barbuy, B. 1988, A&A, 191, 121
Barbuy, B., Perrin, M.-N., Katz, D., et al. 2003, A&A, 404, 661
Barbuy, B., Hill, V., Zoccali, M., et al. 2013, A&A, 559, A5
Barbuy, B., Friaça, A., da Silveira, C. R., et al. 2015, A&A, 580, A40
Barbuy, B., Chiappini, C., & Gerhard, O. 2018, ARA&A, submitted, [arXiv:1805.01142]
Bensby, T., Feltzing, S., & Lundström, I. 2004, A&A, 415, 155
Bensby, T., Yee, J. C., Feltzing, S., et al. 2013, A&A, 549, A147
Bensby, T., Feltzing, S., & Oey, M. S. 2014, A&A, 562, A71
Bensby, T., Feltzing, S., Gould, A., et al. 2017, A&A, 605, A89
Carpenter, J. M. 2001, AJ, 121, 2851
Carretta, E., Bragaglia, A., Gratton, R. G., et al. 2009, A&A, 505, 117
Casey, A. R, & Schlaufman, K. C. 2015, ApJ, 809, 110
Cavichia, O., Mollá, M., Costa, R. D. D., & Maciel, W. J. 2014, MNRAS, 437, 3688
Cayrel, R., Depagne, E., Spite, M., et al. 2004, A&A, 416, 1117
Cescutti, G., Matteucci, F., Lanfranchi, G. A., & McWilliam, A. 2008, A&A, 491, 401
Coelho, P., Barbuy, B., Meléndez, J., Schiavon, R. P., & Castilho, B. V. 2005, A&A, 443, 735
Cooke, R., Pettini, M., Jorgenson, R. A., et al., 2013, MNRAS, 431, 1625
Cooke, R. J., Pettini, M., & Jorgenson, R. A. 2015, ApJ, 800, 12
Cunha, K., & Smith, V. V. 2006, ApJ, 651, 491
Davis, S. P., & Phillips, J. G. 1963, The Red System ($A^2\Pi - X^2\Sigma$) of the CN molecule (Berkeley: University of California Press)
Duffau, S., Caffau, E., Sbordone, L., et al. 2017, A&A, 605, A128

Fenner, Y., Prochaska, J. X., & Gibson, B. K 2004, ApJ, 606, 116
Friaça, A. C. S., & Barbuy, B. 2017, A&A, 598, A121
Fulbright, J. P., McWilliam, A., & Rich, R. M. 2007, ApJ, 661, 1152
Gaia Collaboration (Clementini, G., et al.) 2017, A&A, 605, A79
García-Pérez, A. E., Cunha, K., Shetrone, M., et al. 2013, ApJ, 767, L9
Gonzalez, O. A., Rejkuba, M., Zoccali, M., et al. 2011, A&A, 530, A54
Gustafsson, B., Edvardsson, B., Eriksson, K., et al. 2008, A&A, 486, 951
Hawkins, K., Jofré, P., Masseron, T., & Gilmore, G. 2015, MNRAS, 453, 758
Hill, V., Lecureur, A., Gómez, A., et al. 2011, A&A, 534, A80
Howes, L. M. 2015, PhD Thesis, Australian National University
Howes, L. M., Asplund, M., Casey, A. R., et al. 2014, MNRAS, 445, 4241
Howes, L. M., Casey, A. R., Asplund, M., et al. 2015, Nature, 527, 484
Howes, L. M., Asplund, M., Keller, S. C., et al. 2016, MNRAS, 460, 884
Iben, I. Jr. 1967, ARA&A, 5, 571
Irwin, A. W. 1988, A&AS, 74, 145
Ishigaki, M. N., Aoki, W., & Chiba, M. 2013, ApJ, 771, 67
Johnson, C. I., Rich, R. M., Kobayashi, C., Kunder, A., & Koch, A. 2014, AJ, 148, 67
Jönsson, H., Ryde, N., Schultheis, M., & Zoccali, M. 2017, A&A, 600, A2
Karakas, A. I., & Lattanzio, J. C. 2014, PASA, 31, 30
Kobayashi, C., Umeda, H., Nomoto, K., Tominaga, N., & Ohkubo, T. 2006, ApJ, 643, 1145
Lamb, M., Venn, K., Andersen, D. et al. 2017, MNRAS, 465, 3536
Lecureur, A., Hill, V., Zoccali, M., Barbuy, B., et al. 2007, A&A, 465, 799
McWilliam, A. 2016, PASA, 33, 40
Meléndez, J., Asplund, M., Alves-Brito, A., et al. 2008, A&A, 484, L21
Mikolaitis, S., Hill, V., Recio-Blanco, A., et al. 2014, A&A, 572, A33
Mishenina, T. V., Gorbaneva, T. I., Basak, N. Y., et al. 2011, Astron. Rep. 55, 689
Momany, Y., Vandame, B., Zaggia, S., et al. 2001, A&A, 379, 436
Ness, M., Freeman, K., Athanassoula, E., et al. 2013, MNRAS, 430, 836
Nissen, P. E., & Schuster, W. J. 2011, A&A, 530, A15
Nomoto, K., Tominaga, N., Umeda, H., Kobayashi, C., & Maeda, K. 2006, Nucl. Phys. A, 777, 424
Nomoto, K., Kobayashi, C., & Tominaga, N. 2013, ARA&A, 51, 457
Pettini, M., Ellison, S. L., Steidel, C. C., & Bowen, D. V. 1999, ApJ, 510, 576
Prochaska, J. S., Naumov, S. O., Carney, B. W., McWilliam, A., & Wolfe, A. M. 2000, AJ, 120, 2513
Rafelski, M., Wolfe, A. M., Prochaska, J. X., et al. 2012, ApJ, 755, 89
Rafelski, M., Neeleman, M., Fumagalli, M., et al. 2014, ApJ, 782, L29
Ramírez, I., & Meléndez, J. 2005, ApJ, 626, 465
Reddy, B. E., Lambert, D. L., & Allende Prieto, C. 2006, MNRAS, 367, 1329
Renzini, A., D'Antona, F., Cassisi, S., et al. 2015, MNRAS, 454, 4197
Rich, R. M., & Origlia, L. 2005, ApJ, 634, 1293
Rich, R. M., Origlia, L., & Valenti, E. 2012, ApJ, 746, 59
Rojas-Arriagada, A., Recio-Blanco, A., de Laverny, P., et al. 2017, A&A, 601, A140
Ryde, N., Gustafsson, B., Edvardsson, B., et al. 2010, A&A, 509, A20
Saito, Y.-J., Takada-Hidai, M., Honda, S., & Takeda, Y. 2009, PASJ, 61, 549
Schiavon, R. P., Zamora, O., Carrera, R., et al. 2017, MNRAS, 465, 501
Schlafly, E. F., & Finkbeiner, D. P. 2011, ApJ, 737, 103
Schultheis, M., Rojas-Arriagada, A., García-Pérez, A. E., et al. 2017, A&A, 600, A14
Siqueira-Mello, C., Chiappini, C., Barbuy, B., et al. 2016, A&A, 593, A79
Skúladóttir, Á., Tolstoy, E., Salvadori, S., Hill, V., & Pettini, M. 2017, A&A, 606, A71
Skúladóttir, Á., Salvadori, S., Pettini, M., Tolstoy, E., & Hill, V. 2018, A&A, in press, DOI: 10.1051/0004-6361/201732359
Smiljanic, R., Gauderon, R., North, P., et al. 2009, A&A, 502, 267
Sneden, C., Kraft, R. P., Shetrone, M. D., et al. 1997, AJ, 114, 1964
Steffen, M., Prakapavicius, D., Caffau, E., et al. 2015, A&A, 583, A57
Tsuji, T. 1973, A&A, 23, 411
Udalski, A., Szymanski, M., Kubiak, M., et al. 2002, Acta Astron. 52, 217
Umeda, H., & Nomoto, K. 2002, ApJ, 565, 385
Umeda, H., & Nomoto, K. 2003, Nature, 422, 871
Umeda, H., & Nomoto, K. 2005, ApJ, 619, 427
Vladilo, G., Abate, C., Yin, J., Cescutti, G., & Matteucci, F. 2011, A&A, 530, A33
Wise, J. H., Turk, M. J., Norman, M. L., & Abel, T. 2012, ApJ, 745, 50
Woosley, S. E., & Weaver, T. A. 1995, ApJS, 101, 181
Woosley, S., Heger, A., & Weaver, T. A. 2002, Rev. Mod. Phys., 74, 1015
Zoccali, M., Lecureur, A., Barbuy, B., et al. 2006, A&A, 457, L1
Zoccali, M., Hill, V., Lecureur, A., et al. 2008, A&A, 486, 177
Zoccali, M., Vasquez, S., Gonzalez, O. A., et al. 2017, A&A, 599, A12

Appendix A: Comparison between GIRAFFE and UVES spectra

Figures A.1 present the fits of the Zn I 6362.3 Å line, for both spectra GIRAFFE and UVES for stars in common between the two sets of observations.

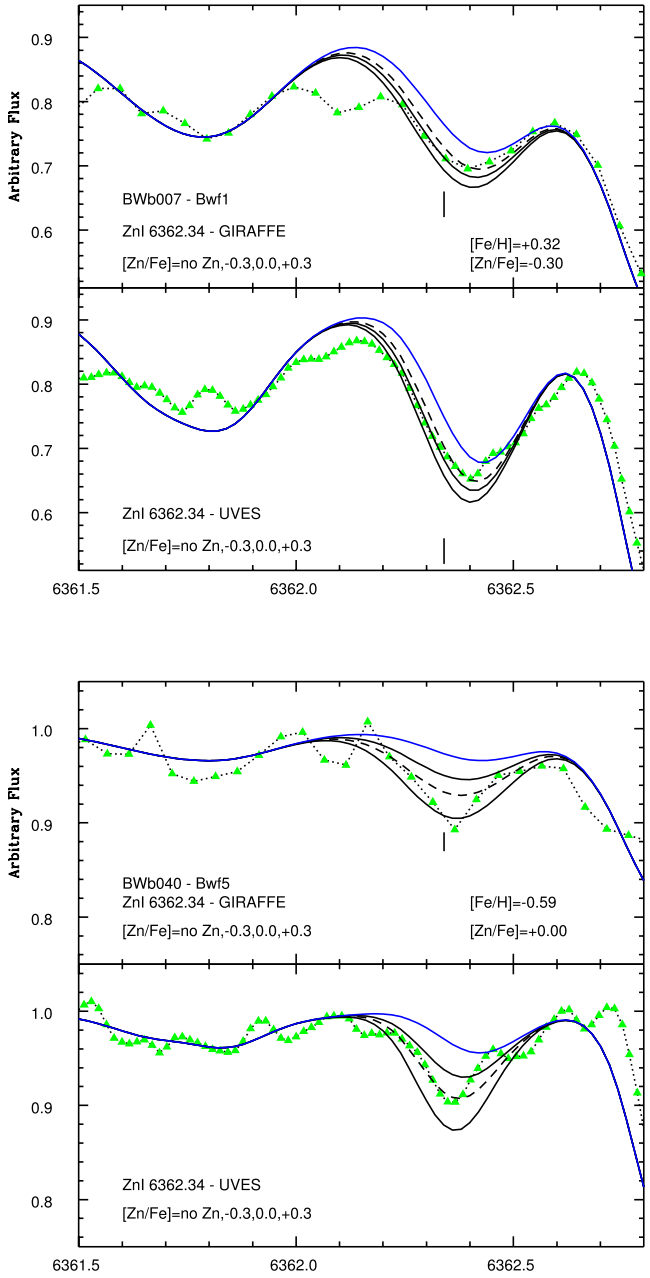

Fig. A.1. Comparison between UVES and Giraffe spectra with fits of the Zn I 6362.3 Å line, for stars in common. Symbols: dotted black line and green filled triangles correspond to the observed spectra: black lines: synthetic spectra, dashed line: synthetic spectrum for the chosen [Zn/Fe] value. Blue solid line: synthetic spectra without Zn, showing the CN line.

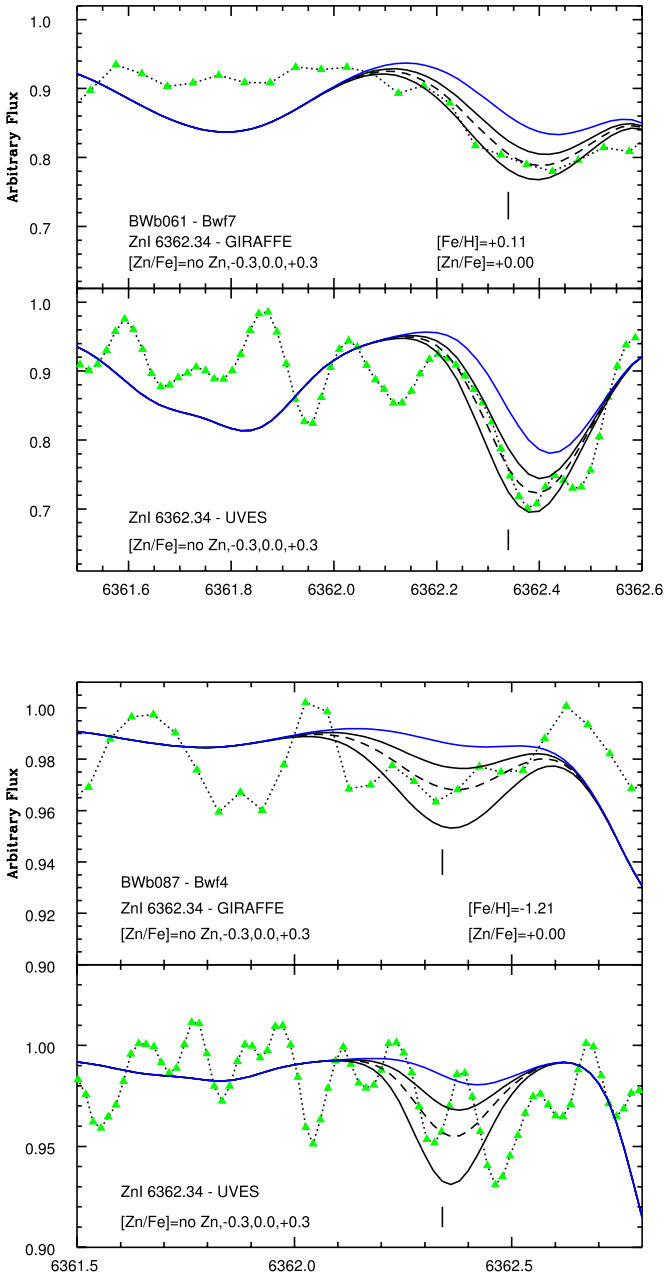

Fig. A.1. continued.

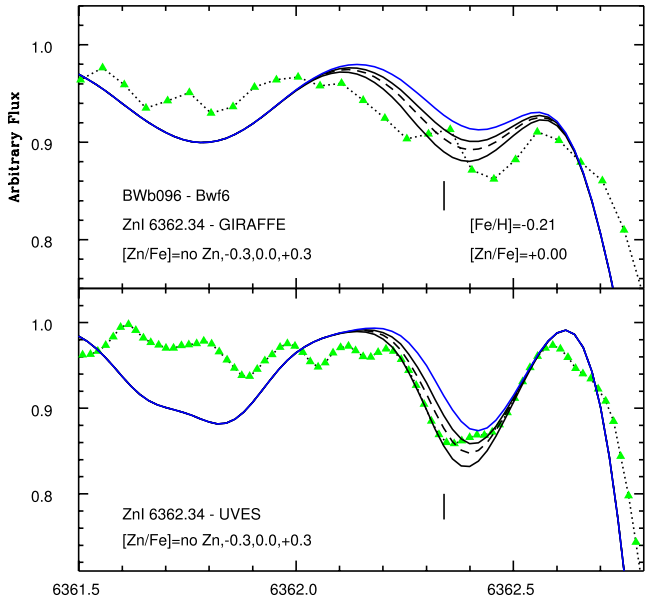

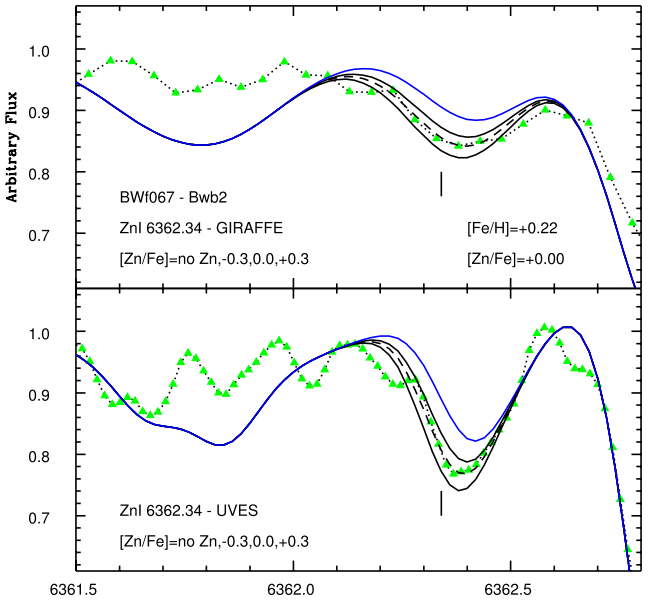

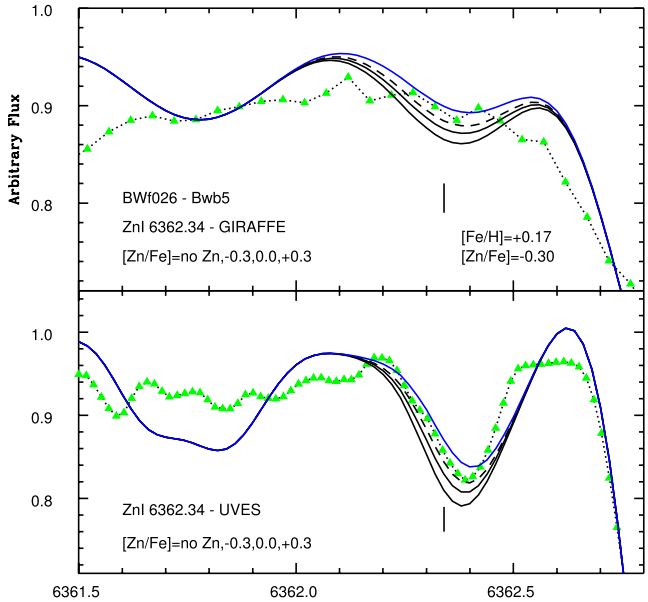

Fig. A.1. continued.

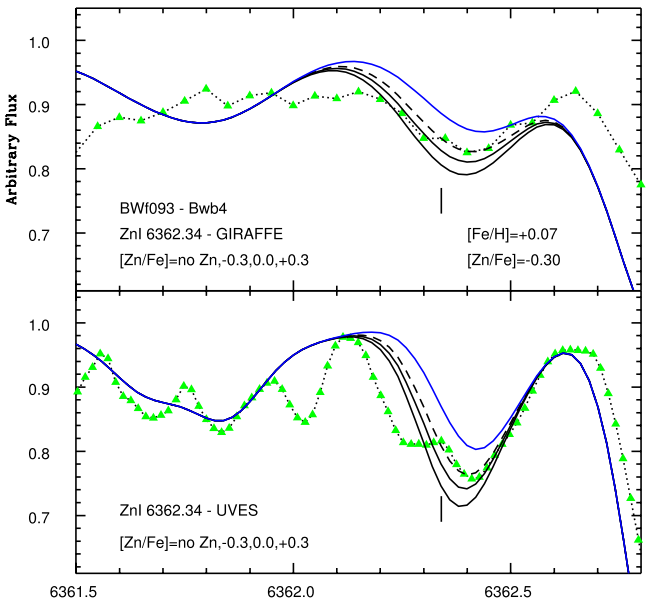

Fig. A.1. continued.

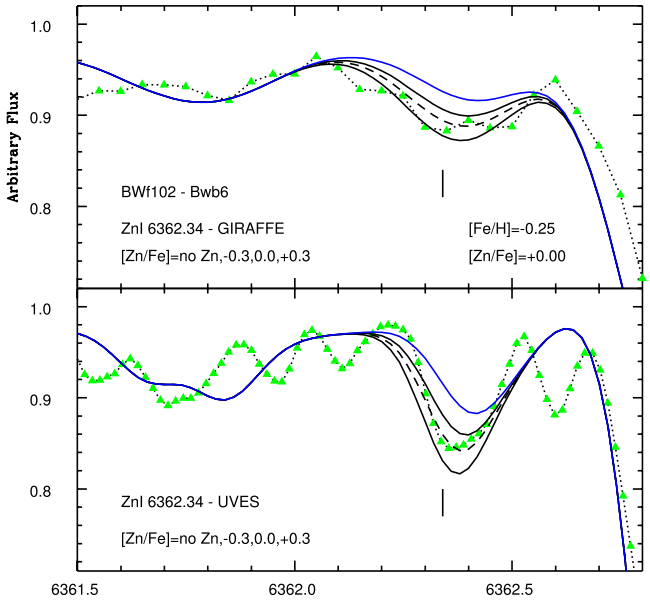

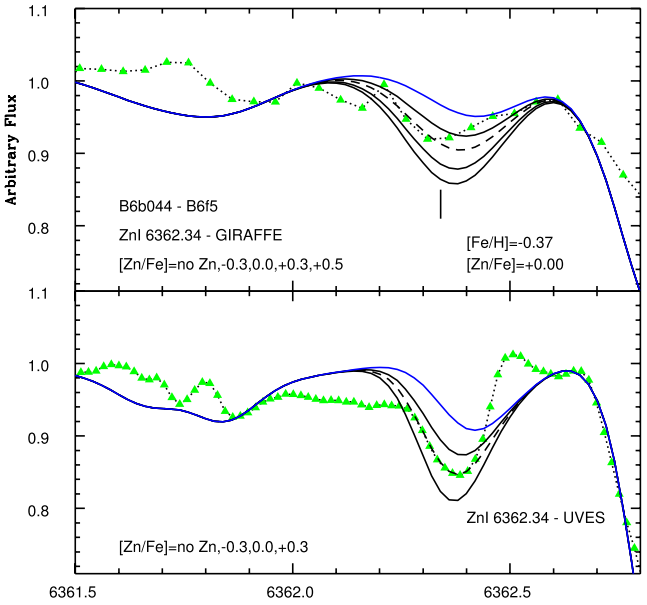

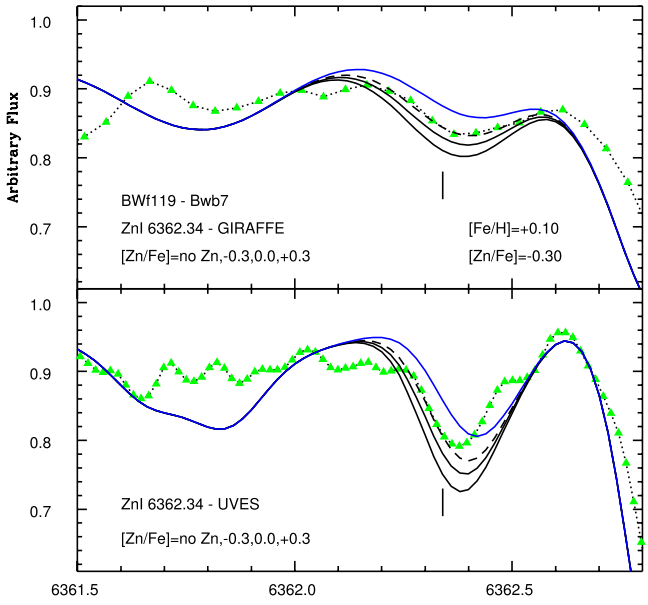

Fig. A.1. continued.

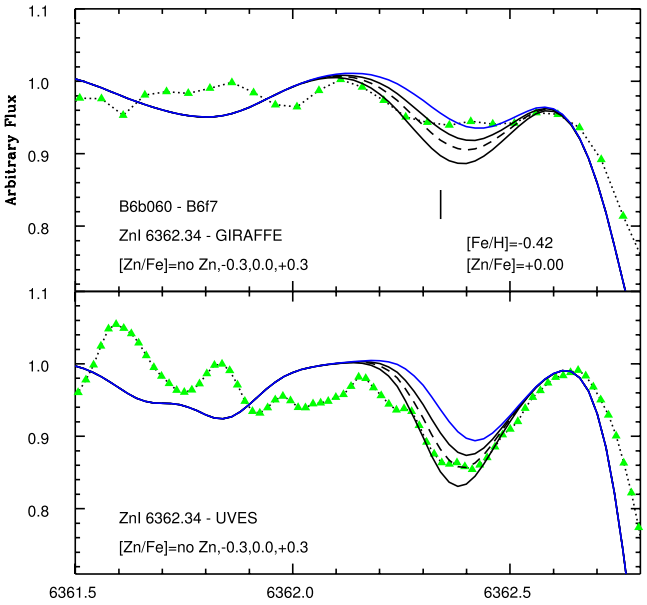

Fig. A.1. continued.

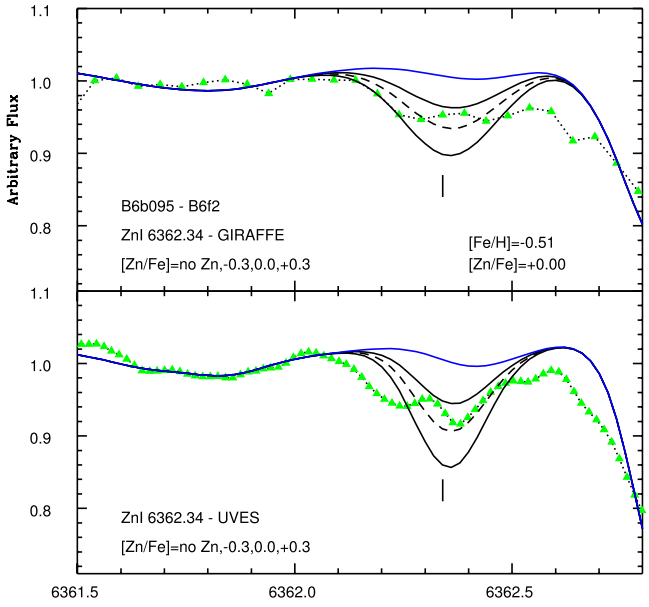

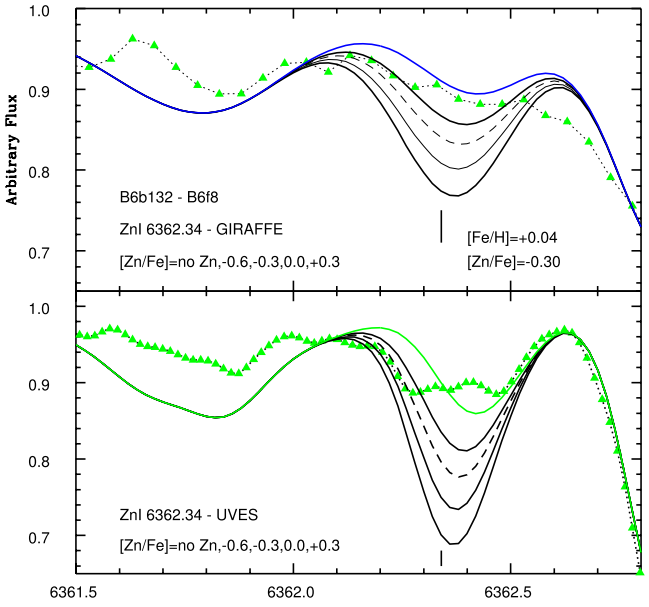

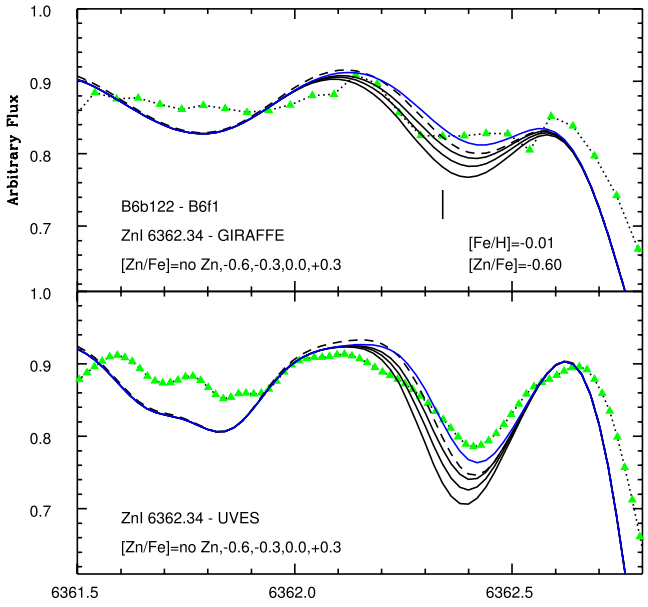

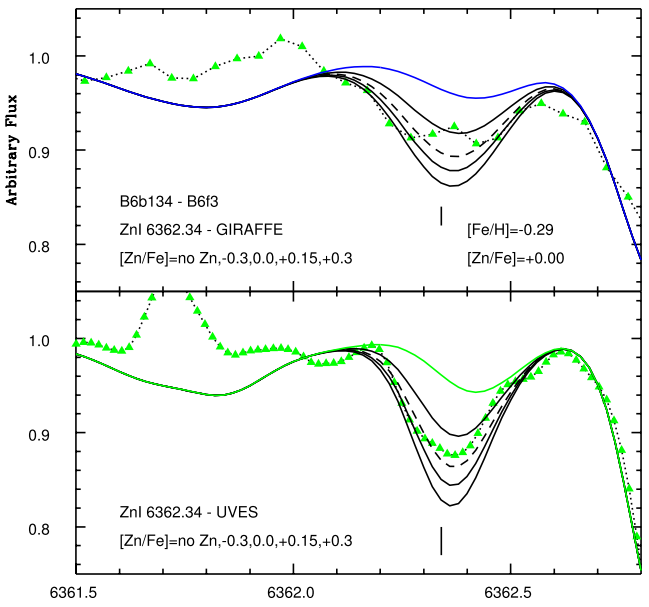

Fig. A.1. continued.

Fig. A.1. continued.

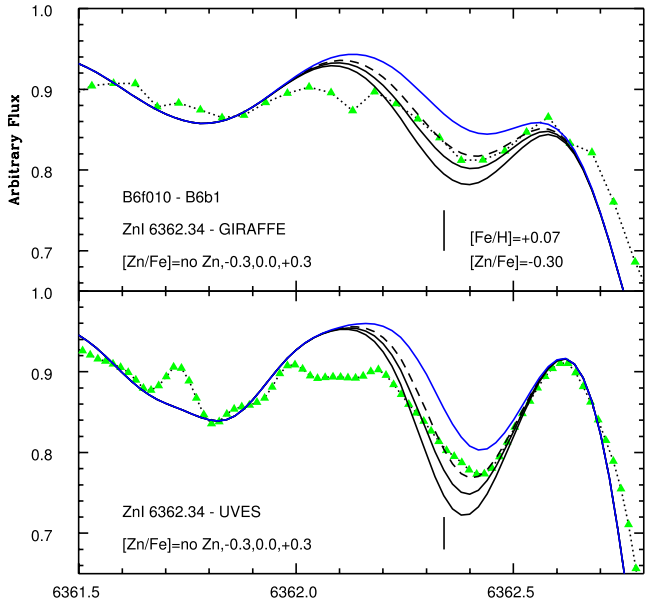

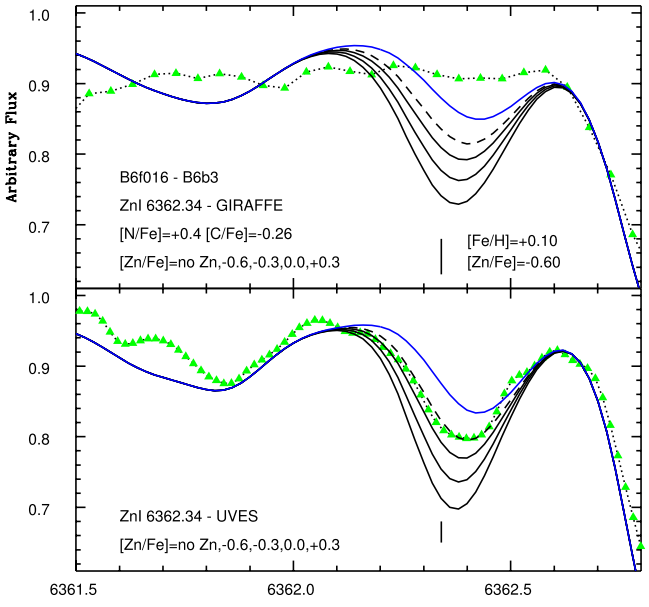

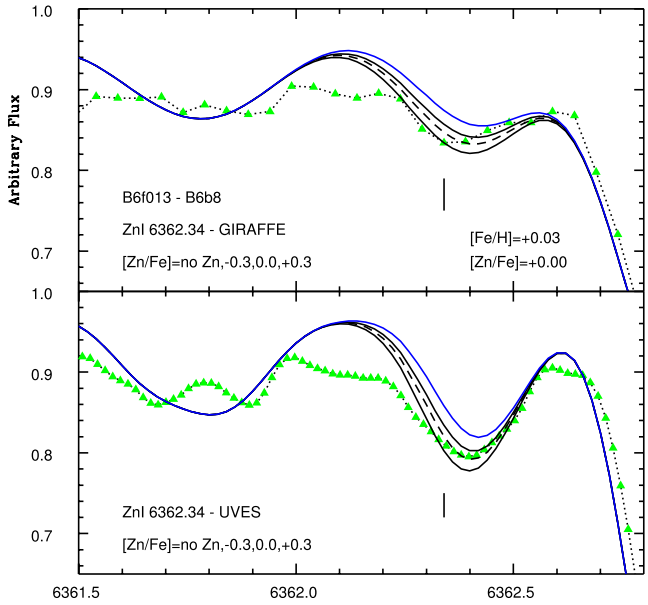

Fig. A.1. continued.

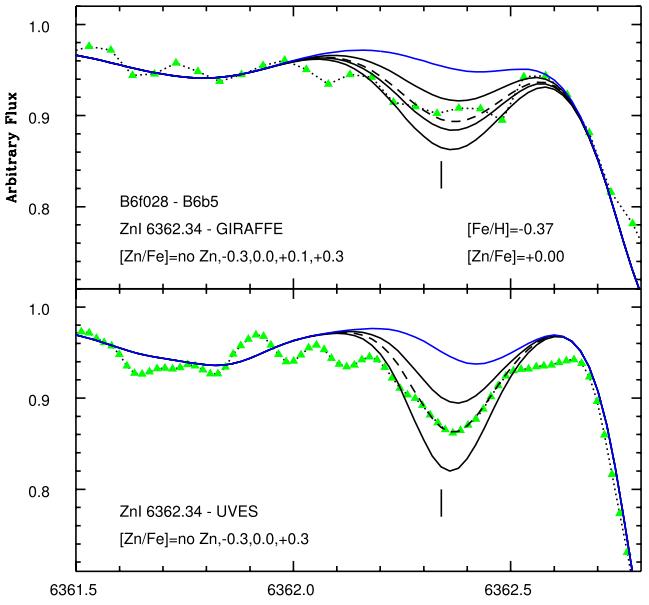

Fig. A.1. continued.

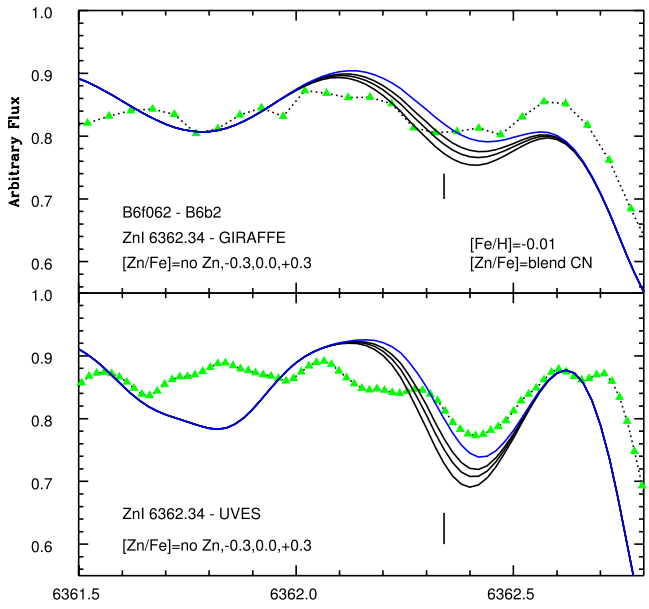

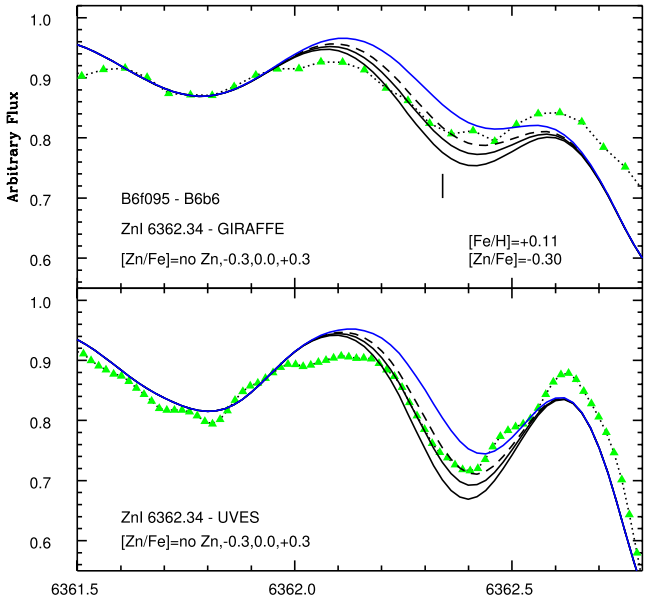

Fig. A.1. continued.

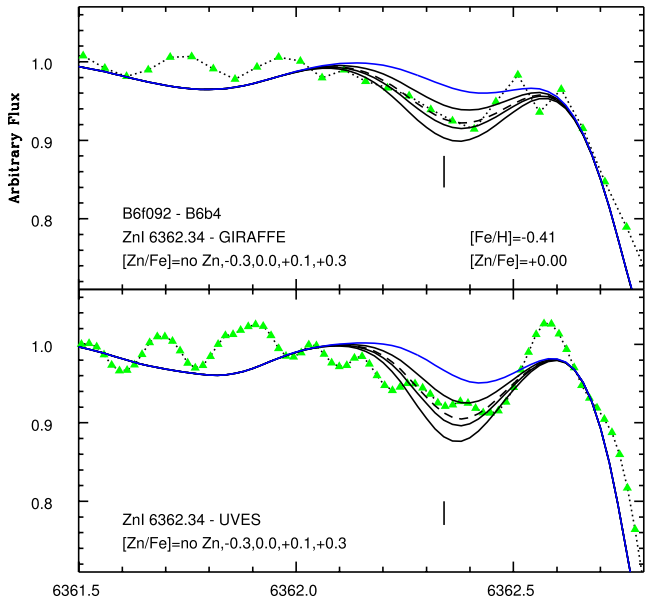

Fig. A.1. continued.

Appendix B: Final abundances.

Table B.1. OGLE and GIRAFFE names, stellar parameters, resulting [N/Fe], [O/Fe], [Zn/Fe], and alpha-element abundances.

OGLE	GIRAFFE	T_{eff}	log g	[Fe/H]	v_t	[N/Fe]	[O/Fe]	[Zn/Fe]	[Mg/Fe]	[Si/Fe]	[Ca/Fe]	[Ti/Fe]
Baade's window bright: BW-f												
423342	bwb002	4650	1.99	0.46	1.3	−0.05	−0.35	−0.30	−0.04	−0.08	0.13	0.03
423323	bwb003	4200	1.59	−0.48	1.5	0.00	0.10	0.22	0.43	0.26	0.15	0.23
412779	bwb004	4850	1.93	−0.37	1.5	0.20	—	0.13	0.23	0.22	0.29	0.48
412803	bwb005	4000	1.52	0.51	1.3	−0.20	−0.35	−0.40	—	—	—	—
423359	bwb006	4650	1.92	−1.23	1.4	—	—	0.30	0.34	0.43	0.30	0.48
433669*	bwb007*	4400	1.80	0.32	1.6	0.45	−0.18	−0.30	−0.02	−0.10	0.01	−0.04
433669	bwb007	4300	1.67	0.32	1.5	0.30	−0.25	−0.40	−0.02	−0.10	0.01	−0.04
412752	bwb008	4900	1.98	−0.80	1.5	1.00	<0.00:	—	0.15	0.30	0.34	0.51
412794	bwb009	4600	1.94	0.13	1.3	0.00	−0.25	0.00	−0.04	−0.08	0.28	0.30
402327	bwb011	4800	2.00	0.15	1.2	0.00	—	−0.03	0.08	−0.17	0.36	0.20
412924	bwb014	4800	2.05	0.48	1.5	0.00	−0.40	−0.33	−0.04	−0.13	0.07	0.17
575317	bwb015	4550	1.78	0.22	1.4	−0.10	−0.35	−0.05	0.14	0.03	0.16	0.07
92600	bwb016	4250	1.70	0.05	1.0	0.50	−0.20	−0.05	0.20	0.08	0.15	0.29
412759	bwb017	4900	1.98	−0.39	1.4	0.30	0.30	0.20	0.24	0.16	0.26	0.31
575356	bwb021	4050	1.56	0.39	1.4	0.05	−0.30	—	—	—	—	—
423331	bwb022	4500	1.88	0.18	1.5	0.10	−0.30	−0.25	−0.02	−0.02	−0.06	−0.14
564797	bwb024	4200	1.69	0.24	1.5	−0.25	−0.30	—	0.02	−0.11	−0.01	0.08
564792	bwb025	5000	2.09	−0.68	1.4	0.00	<0.00:	0.10	0.28	0.30	0.32	0.36
412931	bwb026	4450	1.87	−0.15	1.3	0.20	0.04	0.05	0.25	0.11	0.25	0.31
564988	bwb027	4750	2.04	−0.24	1.4	0.30	0.15	0.30	0.32	0.14	0.19	0.43
412792	bwb030	4450	1.83	−0.26	1.4	0.10	—	0.12	0.29	0.18	0.20	0.43
564762	bwb031	4700	1.87	−0.63	1.6	0.25	0.30	0.15	0.35	0.36	0.19	0.49
564757	bwb033	4800	2.01	0.38	1.3	−0.25	−0.30	−0.15	0.04	−0.08	0.17	−0.07
564807	bwb035	4850	2.00	−0.67	1.5	0.30	0.35	0.15	0.34	0.32	0.26	0.34
575293	bwb037	4450	1.79	0.41	1.3	0.20	−0.25	0.00	0.09	−0.02	0.34	0.11
92537	bwb038	4500	1.81	−0.56	1.3	0.30	0.25	0.15	0.40	0.31	0.37	0.51
575303	bwb039	4850	2.02	−0.27	1.5	—	—	0.10	0.35	0.26	−0.03	0.33
240260*	bwb040*	4800	1.90	−0.59	1.3	0.40	0.25	0.00	0.29	0.09	0.27	0.35
240260	bwb040	5150	2.07	−0.59	1.4	0.45	0.20	0.30	0.29	0.09	0.27	0.35
82762	bwb041	4450	1.81	0.31	1.4	0.05	−0.30	−0.20	0.09	0.01	0.30	−0.06
92565	bwb042	4400	1.84	−0.05	1.5	0.40	—	0.15	0.06	0.01	0.06	0.16
240210	bwb043	4800	2.00	−0.04	1.2	0.30	0.00	0.00	0.23	0.22	0.31	0.28
554722	bwb044	4600	1.67	−0.44	1.6	0.40	0.10	—	0.20	0.26	0.12	0.36
82725	bwb045	4750	1.98	−0.70	1.3	—	—	0.30	0.30	0.41	0.16	0.37
231262	bwb046	4930	2.04	−0.10	1.4	0.30	—	—	0.16	0.10	0.07	0.30
231099	bwb047	5100	2.06	−0.22	1.6	0.30	−0.17	—	0.09	0.09	0.16	0.34
82747	bwb048	5000	2.06	−0.26	1.3	0.00	0.05	—	0.14	0.20	0.27	0.44
63856	bwb049	4700	2.01	0.33	1.3	0.00	−0.25	0.00	0.03	0.00	0.01	−0.06
231144	bwb050	4700	1.94	−0.20	1.5	0.45	0.05	0.10	0.24	0.01	0.22	0.47
231364	bwb053	4800	1.99	0.27	1.5	−0.10	−0.30	—	0.01	−0.11	0.10	0.04
82742	bwb054	4400	1.68	0.17	1.5	0.20	−0.30	−0.30	0.09	0.04	0.03	−0.11
73506	bwb055	4200	1.67	−0.24	1.5	0.50	0.10	—	0.30	0.09	0.10	0.29
222451	bwb056	4750	1.94	−0.33	1.3	−0.10	0.18	0.17	0.22	0.24	0.08	0.32
73504	bwb057	4550	1.92	−0.16	1.4	0.50	0.15	0.10	0.25	0.10	0.20	0.38
82761	bwb058	4800	2.01	−0.21	1.5	0.30	0.25	0.17	0.20	0.13	0.32	0.41
73490	bwb059	4300	1.74	0.49	1.2	−0.40	−0.35	−0.45	0.08	−0.04	0.04	0.00
222618	bwb060	4800	2.03	−0.33	1.4	0.30	0.15	0.10	0.28	0.17	0.31	0.44
357480*	bwb061*	4400	1.90	0.11	1.7	0.70	−0.25	−0.10	−0.12	−0.10	0.08	0.00
357480	bwb061	4800	2.06	0.11	1.4	0.20	−0.25	−0.15	−0.12	−0.10	0.08	0.00
554664	bwb062	4600	1.91	−0.48	1.5	—	0.10	—	0.33	0.31	0.29	0.54
73514	bwb064	4900	2.04	−0.41	1.5	0.50	0.25	0.22	0.35	−0.04	0.29	0.50
205243	bwb065	4900	2.13	0.31	1.4	0.35	−0.30	0.00	0.16	−0.13	0.28	0.30
82705	bwb066	4500	1.80	−0.19	1.4	0.40	0.15	0.17	0.24	0.23	0.32	0.42
205257	bwb068	4600	1.94	−1.10	1.5	0.10	—	0.40	0.29	0.42	0.00	0.19

Notes. For stars having both GIRAFFE and UVES spectra, the parameters from both UVES and GIRAFFE analyses are reported. These stars are marked with an asterisk when corresponding to the UVES results.

Table B.1. continued.

OGLE	GIRAFFE	T_{eff}	log g	[Fe/H]	v_t	[N/Fe]	[O/Fe]	[Zn/Fe]	[Mg/Fe]	[Si/Fe]	[Ca/Fe]	[Ti/Fe]
82831	bwb069	4750	1.99	0.33	1.4	−0.05	−0.35	0.00	0.09	0.07	0.22	0.16
205436	bwb071	5200	2.27	0.16	1.4	0.30	−0.10	−0.20	0.05	−0.10	0.10	0.28
82798	bwb072	5050	2.17	−0.06	1.1	0.40	—	0.15	0.21	0.03	0.26	0.29
73515	bwb073	4550	1.81	−0.45	1.4	0.00	0.10	0.15	0.30	0.18	0.38	0.45
214035	bwb074	4650	1.92	0.26	1.4	0.25	—	−0.30	0.08	−0.01	0.20	0.10
63794	bwb076	4750	2.00	−0.31	1.3	0.50	0.23	0.07	0.16	0.29	0.39	0.31
63792	bwb077	4450	1.82	−0.15	1.3	0.20	0.10	0.10	0.39	0.17	0.25	0.34
54167	bwb078	4800	2.06	−0.38	1.4	0.50	0.10	0.10	0.25	0.41	0.14	0.30
54104	bwb079	4550	1.95	−0.28	1.5	0.60	0.10	0.00	0.28	0.00	0.00	0.20
54132	bwb080	4950	2.06	−0.11	1.4	0.50	0.18	0.00	0.27	0.18	0.11	0.35
54273	bwb081	4850	2.12	0.45	1.3	0.20	−0.35	0.00	—	—	—	—
44560	bwb082	4550	1.93	−0.23	1.4	0.20	0.13	0.00	0.14	0.12	0.16	0.21
205356	bwb083	4950	2.16	−0.19	1.5	0.65	0.15	0.10	0.11	0.17	0.01	0.01
63800	bwb085	4850	1.96	0.31	1.5	0.10	−0.40	−0.20	0.16	−0.14	0.25	0.12
63849	bwb086	4750	1.97	−0.92	1.4	0.30	0.30	0.15	0.35	0.41	0.33	0.48
537070*	bwb087*	4800	1.90	−1.21	1.7	0.70	0.30	0.15	0.38	0.30	0.35	0.49
537070	bwb087	5150	2.14	−1.21	1.1	0.54	0.30	—	0.38	0.30	0.35	0.49
63823	bwb088	4550	1.87	−0.04	1.4	0.20	—	0.15	0.16	0.03	0.07	0.23
545401	bwb090	5150	2.22	0.01	1.4	—	−0.10	−0.05	0.11	0.02	0.18	0.14
545440	bwb091	4500	1.91	−0.60	1.5	0.50	0.40	0.40	0.43	0.34	0.31	0.30
54311	bwb092	4900	2.15	0.26	1.5	−0.05	−0.30	0.00	0.06	−0.03	0.09	0.22
537101	bwb093	4800	2.07	−0.67	1.3	0.80	0.30	0.15	0.14	0.31	0.28	0.23
554655	bwb095	4900	2.03	−0.34	1.5	0.40	—	0.08	0.13	0.17	0.11	0.24
392918*	bwb096*	4100	1.70	−0.21	1.5	0.40	0.20	0.08	0.11	0.10	0.24	0.32
392918	bwb096	4600	1.97	−0.21	1.4	0.30	0.08	0.22	0.11	0.10	0.24	0.32
63839	bwb097	4300	1.74	−0.22	1.4	0.30	0.20	0.10	0.24	0.09	0.21	0.25
554700	bwb098	4900	2.02	−0.17	1.4	0.20	—	0.05	0.11	0.15	0.14	0.31
554787	bwb099	4700	2.04	−0.58	1.2	0.00	0.15	0.18	0.31	0.31	0.39	0.36
63855	bwb100	4200	1.67	0.40	1.4	−0.45	−0.35	−0.40	0.14	0.10	−0.04	−0.04
63850	bwb101	4600	1.78	-1.61	1.6	0.00	0.35	0.40	—	—	—	—
402294	bwb102	4800	2.05	−0.50	1.2	0.50	0.20	0.15	0.43	0.31	0.38	0.53
63820	bwb103	5100	2.19	−0.14	1.2	0.20	−0.10	0.08	0.11	0.10	0.31	0.27
393015	bwb104	4850	2.09	−0.06	1.3	0.20	0.02	0.02	0.41	0.02	0.36	0.35
554663	bwb105	4700	1.86	−0.72	1.3	0.40	0.35	0.22	0.40	0.44	0.36	0.33
63834	bwb106	4950	2.08	0.16	1.4	0.20	−0.30	−0.20	0.21	0.01	0.19	0.25
402361	bwb107	4950	2.00	−1.05	1.4	0.00	0.28	0.22	0.24	0.41	0.30	0.40
402307	bwb109	4600	1.93	0.40	1.5	−0.05	−0.40	−0.30	0.05	−0.11	0.17	0.10
402414	bwb110	4650	1.99	−0.21	1.4	0.20	−0.10	−0.20	0.39	0.29	0.11	0.49
545288	bwb111	4600	1.94	0.13	1.3	0.20	−0.30	−0.20	0.19	0.11	0.20	0.15
554889	bwb112	5000	2.18	−0.10	1.3	0.30	−0.10	−0.10	0.12	0.13	0.33	0.30
402315	bwb113	4750	1.97	−0.17	1.4	0.20	0.00	0.14	0.25	0.08	0.31	0.41
554811	bwb114	4900	2.11	0.17	1.3	0.15	−0.25	−0.15	0.04	0.00	0.30	0.05
234671	bwb115	4500	1.86	0.06	1.4	−0.15	−0.10	−0.10	0.04	−0.03	0.05	0.05
402332	bwb117	4500	1.82	−0.31	1.4	0.30	0.10	0.25	0.26	0.28	0.19	0.41
402322	bwb118	4800	1.94	−0.94	1.5	0.00	—	0.32	0.36	0.32	0.36	0.35
564743	bwb119	4250	1.70	0.21	1.4	0.20	−0.20	—	0.12	−0.04	0.03	0.06
402311	bwb120	4500	1.89	0.08	1.5	0.00	−0.20	0.10	0.12	0.00	0.15	0.26
244582	bwb122	4950	2.01	−0.81	1.3	0.70	<−0.05:	0.30	0.21	0.20	0.33	0.30
244504	bwb123	4550	1.83	−0.25	1.4	0.30	0.15	0.10	0.26	0.27	0.22	0.35
402607	bwb128	4800	2.04	−0.82	1.3	0.70	<0.00:	0.35	0.23	0.39	0.28	0.40
402531	bwb130	5100	2.21	−0.85	1.2	0.70	<0.10:	0.12	0.26	0.36	0.28	0.51
402325	bwb132	4500	1.87	−0.32	1.4	0.50	0.15	0.05	0.23	0.29	0.13	0.36
256308	bwb135	4800	1.95	−1.69	1.4	—	—	—	—	—	—	—

Table B.1. continued.

OGLE	GIRAFFE	T_{eff}	log g	[Fe/H]	v_t	[N/Fe]	[O/Fe]	[Zn/Fe]	[Mg/Fe]	[Si/Fe]	[Ca/Fe]	[Ti/Fe]
Baade's window faint: BW-f												
585982	bwf003	4600	1.99	−0.08	1.4	0.20	−0.05	0.03	0.41	0.09	0.15	0.28
575308	bwf004	4350	1.84	0.27	1.4	0.10	−0.25	—	0.16	0.08	0.26	0.27
575289	bwf005	4450	1.92	−0.50	1.5	0.20	—	—	0.49	0.21	0.29	0.45
423298	bwf007	4400	1.91	−0.08	1.2	0.50	−0.05	0.05	0.12	0.20	0.28	0.24
433830	bwf008	4200	1.87	0.18	1.5	0.20	−0.25	−0.25	0.25	−0.04	−0.08	0.00
564963	bwf009	4250	1.83	0.34	1.0	0.30	−0.30	−0.35	0.19	−0.05	0.14	0.14
554980	bwf010	4600	1.99	0.31	1.5	0.00	−0.40	−0.40	0.03	−0.18	0.03	0.08
423304	bwf013	4350	2.03	0.22	1.4	0.15	−0.30	−0.10	0.02	−0.09	0.06	0.24
102833	bwf014	4500	2.05	0.29	1.5	−0.10	−0.40	−0.15	0.11	−0.15	0.24	0.17
102853	bwf015	4400	1.86	0.15	1.2	0.45	−0.20	—	0.14	0.00	0.27	0.27
564768	bwf016	4150	1.74	−0.30	1.3	0.50	0.15	0.13	0.06	0.28	0.28	0.42
586077	bwf017	4500	2.02	0.21	1.3	−0.05	−0.30	−0.22	0.07	−0.16	0.04	0.08
586005	bwf018	4400	1.91	0.29	1.3	0.10	−0.30	—	0.00	−0.18	0.08	0.09
564789	bwf019	4100	1.70	−0.15	1.2	0.30	0.10	0.05	0.03	0.04	0.10	0.42
596502	bwf020	4150	1.87	0.28	1.1	0.35	−0.25	—	0.19	0.10	0.03	0.10
575360	bwf021	4500	1.96	−0.05	1.2	0.60	−0.10	—	—	—	—	—
564991	bwf022	4400	1.98	0.19	1.4	0.25	−0.30	—	0.05	0.00	0.09	0.19
82760*	bwf026*	4000	1.60	0.17	1.2	0.05	−0.10	−0.30	−0.06	−0.20	−0.05	0.03
82760	bwf026	4300	1.87	0.17	1.5	0.00	0.00	—	−0.06	−0.20	−0.05	0.03
82727	bwf028	4200	1.78	0.17	1.3	0.55	−0.15	−0.05	0.05	−0.16	0.15	0.11
92557	bwf029	4700	2.05	−0.07	1.4	0.15	0.10	0.00	0.18	−0.05	0.18	0.46
231128	bwf033	4200	1.76	0.17	1.4	−0.10	−0.30	−0.05	−0.03	−0.08	0.03	0.10
82717	bwf034	4150	1.77	0.28	1.1	−0.10	−0.35	—	0.15	−0.18	−0.03	0.18
240216	bwf035	4400	1.86	0.19	1.2	0.35	−0.20	−0.15	0.11	0.04	0.31	0.21
240459	bwf036	4550	2.02	−0.39	1.2	0.20	0.15	—	0.31	0.41	0.28	0.54
240394	bwf037	4600	2.04	0.14	1.6	0.40	−0.20	—	0.16	−0.08	0.04	0.01
231369	bwf038	4200	1.82	0.29	1.5	0.40	−0.20	—	0.07	−0.16	0.01	−0.01
231367	bwf040	4600	2.00	−0.01	1.4	0.00	−0.10	−0.15	0.11	0.01	0.12	0.27
231310	bwf041	4500	1.95	0.30	1.1	−0.05	−0.30	−0.25	0.11	−0.10	0.31	0.08
374186	bwf042	4350	1.96	0.20	1.2	0.35	−0.25	—	0.05	0.04	0.08	0.17
231325	bwf043	4200	1.81	0.34	1.5	−0.15	−0.35	—	−0.11	0.00	−0.09	0.05
222627	bwf046	4100	1.78	0.13	1.1	0.45	−0.20	—	0.13	0.03	0.13	0.08
231185	bwf049	4500	1.98	0.19	1.3	0.15	−0.20	−0.15	−0.04	−0.10	0.21	0.15
231233	bwf051	4550	1.97	−0.16	1.3	0.30	0.00	−0.05	0.26	0.12	0.13	0.08
365797	bwf053	4550	1.95	−0.19	1.3	0.60	—	0.12	0.34	0.17	0.26	0.56
222412	bwf054	4400	1.86	−0.11	1.3	0.30	0.13	0.20	0.20	0.17	0.28	0.46
222408	bwf055	4100	1.72	0.31	1.5	0.20	−0.30	—	0.25	0.00	0.04	0.03
357466	bwf056	4300	1.98	0.43	1.3	−0.50	−0.35	−0.50	0.07	0.01	−0.09	0.27
350527	bwf057	4600	2.04	−0.65	1.4	0.40	—	—	0.37	0.30	0.33	0.56
222523	bwf059	4250	1.88	0.01	1.4	0.15	−0.08	0.05	0.24	0.30	−0.03	0.09
222543	bwf060	4350	1.99	0.34	1.1	0.00	−0.32	−0.40	−0.12	−0.04	0.14	0.18
357436	bwf061	4500	1.95	0.44	1.3	−0.30	−0.40	—	−0.10	−0.09	0.13	0.01
357459	bwf062	4600	2.08	−0.01	1.5	0.35	0.00	—	0.06	0.04	0.10	0.29
73607	bwf064	4600	2.00	0.28	1.2	0.20	−0.30	−0.15	0.07	−0.01	0.03	0.13
73483	bwf065	4300	1.87	0.16	1.4	0.30	−0.20	—	0.01	0.02	0.04	0.08
73609	bwf066	4300	1.91	0.28	1.5	0.25	−0.20	—	0.03	−0.09	−0.10	0.08
214192*	bwf067*	4300	1.90	0.22	1.5	0.20	−0.10	−0.15	0.22	−0.02	0.18	0.24
214192	bwf067	4450	1.96	0.22	1.3	0.15	−0.10	−0.20	0.22	−0.02	0.18	0.24
73472	bwf069	4400	1.98	0.49	1.5	−0.20	−0.32	—	−0.17	−0.25	0.01	0.02
64005	bwf070	4500	1.99	−0.25	1.4	0.35	0.18	0.15	0.36	0.16	0.17	0.39
205265	bwf071	4500	1.94	0.02	1.3	0.20	−0.10	—	0.03	0.03	0.16	0.33
214042	bwf072	4150	1.76	0.38	1.3	−0.25	−0.35	−0.40	0.14	−0.06	0.08	−0.01
350483	bwf073	4200	1.87	0.14	1.3	0.45	−0.15	−0.05	0.13	0.03	0.09	0.13
64018	bwf074	4500	1.92	0.15	1.5	0.20	−0.28	−0.15	0.12	0.22	0.08	0.01
63859	bwf075	4400	1.86	0.25	1.5	0.30	−0.25	—	0.23	0.00	0.11	0.13
545445	bwf076	4550	2.01	0.13	1.5	0.00	−0.20	−0.18	−0.01	0.01	0.02	0.05

Table B.1. continued.

OGLE	GIRAFFE	T_{eff}	log g	[Fe/H]	v_t	[N/Fe]	[O/Fe]	[Zn/Fe]	[Mg/Fe]	[Si/Fe]	[Ca/Fe]	[Ti/Fe]
63840	bwf077	4500	1.99	0.31	1.1	0.15	−0.35	−0.60	0.15	−0.01	0.22	0.19
54108	bwf078	4400	1.91	0.46	1.5	−0.30	−0.30	−0.55	−0.09	−0.26	−0.02	0.03
54125	bwf079	4400	2.00	0.07	1.3	0.35	−0.15	—	0.18	0.22	0.19	0.28
73467	bwf080	4250	2.00	0.12	1.4	−0.30	−0.23	−0.20	0.08	−0.02	0.01	0.19
54133	bwf081	4050	1.67	0.35	1.0	−0.10	−0.33	−0.45	—	—	—	—
54078	bwf082	4350	1.89	0.09	1.5	0.30	−0.20	−0.15	0.01	−0.01	0.26	0.08
63829	bwf083	4400	2.01	−0.01	1.5	0.80	−0.10	—	0.17	0.01	0.06	0.09
537095	bwf085	4500	1.93	0.31	1.2	0.00	−0.40	−0.40	0.05	0.00	0.17	0.04
545222	bwf086	4300	1.78	0.16	1.4	0.20	−0.20	−0.10	0.12	0.02	0.12	0.19
545438	bwf087	4350	1.97	0.12	1.5	0.30	−0.12	−0.15	0.16	−0.04	0.05	0.19
545233	bwf088	4350	1.88	0.31	1.3	−0.10	−0.35	—	0.07	−0.03	0.09	0.17
545313	bwf091	4400	2.05	0.16	1.4	−0.20	−0.13	−0.20	0.16	−0.05	−0.08	0.30
537092	bwf092	4600	2.03	−0.25	1.0	0.20	0.15	0.10	0.39	0.00	0.33	0.46
545277*	bwf093*	4300	1.40	0.07	1.4	0.00	−0.10	−0.45	—	—	—	—
545277	bwf093	4100	1.84	0.07	1.2	−0.10	−0.20	—	—	—	—	—
402415	bwf095	4600	2.08	0.01	1.2	0.10	−0.10	—	0.18	−0.05	0.00	0.31
554670	bwf096	4150	1.75	−0.26	1.3	0.35	0.13	0.25	0.25	0.26	0.18	0.48
554748	bwf097	4600	1.99	0.39	1.3	0.15	−0.40	—	0.07	−0.08	0.01	0.09
392952	bwf098	4200	1.79	0.13	1.5	0.40	−0.15	—	0.16	−0.14	0.12	0.09
392896	bwf099	4200	1.80	−0.12	1.3	0.70	0.15	0.05	0.20	0.16	0.06	0.38
393083	bwf100	4450	1.98	0.03	1.5	0.10	−0.05	0.00	0.19	−0.02	0.02	0.22
393053	bwf101	4250	1.83	0.49	1.2	−0.45	−0.38	−0.25	0.09	−0.15	0.04	0.03
392931*	bwf102*	4200	1.70	−0.25	1.3	0.65	0.15	0.00	0.19	−0.03	0.03	0.09
392931	bwf102	4450	1.89	−0.25	1.5	0.70	0.10	0.20	0.19	−0.03	0.03	0.09
545269	bwf103	4250	1.83	0.45	1.1	−0.50	−0.35	—	0.09	−0.09	0.04	0.06
554683	bwf104	4500	2.00	−0.20	1.2	0.30	0.20	0.17	0.21	0.11	0.31	0.49
554668	bwf105	4300	1.85	0.08	1.3	0.30	−0.20	—	0.17	0.03	0.04	0.17
78106	bwf107	4300	1.98	−0.17	1.2	0.50	0.20	0.05	0.40	0.11	0.19	0.49
402498	bwf108	4450	1.90	0.55	1.2	−0.40	−0.40	—	0.06	−0.18	0.05	−0.05
234704	bwf109	4500	1.93	−0.18	1.4	0.10	0.20	0.17	0.26	0.09	0.21	0.36
67494	bwf110	4650	2.02	−0.05	1.1	−0.10	0.05	—	—	—	—	—
234701	bwf111	4500	1.98	0.12	1.2	0.45	−0.20	−0.05	0.24	−0.05	0.27	0.26
234888	bwf112	4200	1.94	0.28	1.5	−0.10	−0.35	—	−0.60	−0.17	0.03	0.00
554713	bwf113	4250	1.90	0.20	1.4	0.20	−0.25	—	0.16	0.05	0.09	0.13
554956	bwf114	4600	1.99	−0.01	1.1	0.40	0.05	−0.12	0.19	0.03	0.30	0.49
392951	bwf115	4650	2.10	0.10	1.3	0.45	−0.30	—	0.11	−0.17	0.04	0.32
412750	bwf116	4350	1.83	0.11	1.1	0.25	−0.10	−0.05	0.14	−0.04	0.25	0.29
411479	bwf117	5200	2.32	−0.30	1.2	—	0.00	0.00	0.09	0.23	0.34	0.39
402656	bwf118	4750	2.08	−0.32	1.2	0.50	0.20	0.15	0.31	0.10	0.33	0.54
554694*	bwf119*	4200	1.40	0.10	1.2	0.10	−0.20	−0.30	0.07	0.05	0.04	0.31
554694	bwf119	4300	1.89	0.10	1.2	0.10	−0.20	−0.10	0.07	0.05	0.04	0.31
402375	bwf120	4200	1.80	0.05	1.4	0.40	−0.15	—	0.22	0.02	0.20	0.25
244829	bwf121	4800	2.09	−1.09	1.4	0.30	0.23	0.35	0.43	0.47	0.36	0.50
402353	bwf122	4800	2.27	0.01	1.5	0.55	−0.15	—	—	—	—	—
244738	bwf123	4800	2.12	−0.25	1.3	0.30	0.23	0.10	0.27	0.08	0.34	0.48
402347	bwf124	4200	1.82	0.19	1.2	0.05	−0.25	—	0.06	−0.04	0.03	0.39
564772	bwf126	4300	1.92	−0.07	1.5	0.50	−0.10	0.00	0.21	0.15	0.06	0.33
423286	bwf128	4350	1.90	0.05	1.2	0.35	−0.15	—	0.11	0.04	0.18	0.29
267974	bwf129	4400	1.94	0.31	1.2	0.05	−0.30	—	−0.04	−0.19	0.07	0.18
412753	bwf133	4300	1.84	0.33	1.1	−0.30	−0.35	—	0.09	−0.17	0.09	0.21
256345	bwf134	4250	1.78	0.33	1.5	−0.05	−0.30	—	0.06	0.00	0.04	0.02

Table B.1. continued.

OGLE	GIRAFFE	T_{eff}	log g	[Fe/H]	v_t	[N/Fe]	[O/Fe]	[Zn/Fe]	[Mg/Fe]	[Si/Fe]	[Ca/Fe]	[Ti/Fe]
Field at −6° bright: B6-b												
41958c3	b6b002	5100	2.04	0.05	1.5	0.45	−0.27	−0.32	0.20	−0.10	0.11	0.32
157820c3	b6b003	4800	1.87	−0.73	1.6	0.40	0.25	0.20	0.40	0.27	0.25	0.37
32799c3	b6b004	4850	2.04	−1.25	1.5	0.00	—	0.55	0.44	0.40	0.22	0.29
76187c3	b6b005	4550	1.79	−0.42	1.6	0.35	0.15	0.15	0.44	0.26	0.26	0.48
38354c3	b6b006	4700	1.83	−0.61	1.7	0.40	0.20	0.25	0.33	0.22	0.29	0.43
203158c3	b6b007	4800	1.86	−0.04	1.6	0.30	−0.12	0.05	0.29	0.01	0.09	0.38
39802c3	b6b008	5200	2.17	−0.50	1.6	—	—	0.10	0.17	0.18	0.22	0.26
43054c3	b6b009	4800	2.01	−1.03	1.5	0.50	0.35	0.35	0.32	0.44	0.29	0.33
46885c3	b6b010	4350	1.70	0.00	1.5	0.50	0.00	0.04	0.15	0.10	0.17	0.04
1604c2	b6b011	4700	1.92	−1.13	1.4	1.00	—	0.45	0.38	0.46	0.39	0.47
36989c3	b6b012	4700	1.88	0.05	1.5	0.15	−0.23	−0.08	0.23	0.09	0.10	0.12
36067c3	b6b013	4550	1.78	0.08	1.4	0.25	−0.08	0.20	0.19	0.12	0.09	0.15
77454c2	b6b015	4950	1.95	−0.38	1.6	0.50	0.25	0.20	0.30	0.10	0.20	0.31
43562c2	b6b016	4600	1.84	−0.81	1.7	0.70	—	0.45	0.37	0.40	0.18	0.34
32832c2	b6b017	4350	1.71	−0.03	1.5	0.50	—	—	0.17	−0.01	0.09	0.19
62009c2	b6b018	4350	1.73	−0.39	1.5	0.30	0.05	0.10	0.37	0.37	0.21	0.36
38565c2	b6b019	4600	1.87	−0.26	1.7	0.35	0.05	0.12	0.27	0.08	0.13	0.42
204270c3	b6b020	4900	2.05	0.02	1.3	0.10	−0.02	0.18	0.25	−0.02	0.28	0.20
69429c3	b6b021	4500	1.79	−0.76	1.5	0.70	0.30	—	0.41	0.39	0.24	0.36
56671c3	b6b022	4900	1.98	−0.20	1.3	0.30	0.05	0.17	0.24	0.11	0.30	0.14
25213c2	b6b023	4600	1.87	0.09	1.5	0.35	−0.15	−0.20	0.14	0.06	0.05	0.03
35428c2	b6b024	4800	1.92	−1.16	1.6	0.50	0.30	0.26	0.13	0.35	0.24	0.40
31338c2	b6b026	4700	1.89	−0.55	1.6	0.15	0.25	—	0.28	0.20	0.10	0.49
53477c2	b6b028	4650	1.85	−0.55	1.6	0.30	0.25	0.22	0.30	0.22	0.28	0.40
56410c2	b6b029	4600	1.81	−1.10	1.5	0.30	—	0.35	0.41	0.30	0.26	0.30
4799c2	b6b030	4950	2.10	−0.12	1.2	0.30	−0.15	0.05	0.26	0.26	0.41	0.42
43239c2	b6b031	5200	2.19	−1.26	1.6	0.00	—	0.28	0.31	0.30	0.20	0.46
14297c2	b6b033	4900	2.01	−0.66	1.8	0.40	0.30	0.30	0.51	0.29	0.11	0.41
17437c2	b6b034	4800	1.97	−0.50	1.6	0.70	0.25	0.33	0.39	0.25	0.29	0.53
41995c2	b6b035	4800	1.98	−1.58	2.0	—	—	—	—	—	—	—
30173c2	b6b036	4900	2.05	−0.90	1.7	0.40	—	0.38	0.21	0.38	0.23	0.44
45160c2	b6b037	4700	1.91	−0.56	1.5	0.40	0.28	0.20	0.41	0.09	0.32	0.47
13661c2	b6b038	4850	1.98	−0.09	1.5	0.30	−0.05	0.02	0.20	0.04	0.14	0.25
212324c6	b6b039	4800	1.88	−0.32	1.2	0.40	0.10	0.10	0.35	0.10	0.39	0.41
10381c2	b6b040	4700	1.90	−0.14	1.3	0.30	—	0.08	0.11	0.30	0.23	0.25
14893c2	b6b041	4050	1.51	−0.47	1.5	0.40	0.15	0.35	0.34	0.36	0.05	0.16
204828c2	b6b042	5000	2.10	−0.22	1.5	0.20	0.00	0.00	0.27	0.11	0.27	0.38
203913c2	b6b043	4900	1.93	−0.24	1.5	0.40	0.15	0.12	0.35	0.08	0.29	0.30
33058c2*	b6b044*	4500	1.80	−0.37	1.4	0.00	0.10	0.05	0.41	0.09	0.26	0.40
33058c2	b6b044	4550	1.84	−0.37	1.7	0.40	0.00	0.08	0.41	0.09	0.26	0.40
212175c6	b6b045	4650	1.90	−0.47	1.5	0.40	0.27	0.08	0.38	0.26	0.33	0.55
213150c6	b6b046	4300	1.67	−0.02	1.5	0.25	−0.12	0.00	0.06	0.07	−0.04	0.16
1678c2	b6b048	4900	1.98	−0.95	1.8	0.50	0.33	0.25	−0.03	0.30	0.22	0.40
874c2	b6b049	4550	1.84	−0.32	1.5	0.60	0.20	0.17	0.32	0.00	0.24	0.42
7694c2	b6b050	5100	2.11	0.15	1.9	0.40	−0.35	−0.24	0.09	−0.04	0.06	0.19
8312c2	b6b051	5000	2.07	−0.32	2.0	0.40	−0.05	0.08	0.17	0.22	0.11	0.25
19402c1	b6b052	4550	1.83	−0.61	1.5	0.45	0.25	0.40	0.32	0.20	0.29	0.38
23483c1	b6b053	5150	2.01	−0.52	1.4	0.30	—	0.17	0.33	0.24	0.38	0.31
98692c6	b6b054	5000	2.22	0.07	1.4	0.30	−0.25	−0.32	0.17	−0.03	0.23	0.30
94324c6	b6b055	4700	1.90	−0.39	1.6	0.20	0.20	0.18	0.38	0.19	0.28	0.51
99147c5	b6b056	4550	1.86	−0.60	1.6	0.25	—	0.25	0.29	0.29	0.13	0.38
96158c6	b6b058	5000	2.10	−0.37	1.4	0.30	<−0.30:	0.15	0.35	0.16	0.31	0.54
100047c6*	b6b060*	4300	1.70	−0.42	1.6	0.30	0.25	−0.08	0.31	0.14	0.14	0.43

Table B.1. continued.

OGLE	GIRAFFE	T_{eff}	log g	[Fe/H]	v_t	[N/Fe]	[O/Fe]	[Zn/Fe]	[Mg/Fe]	[Si/Fe]	[Ca/Fe]	[Ti/Fe]
100047c6	b6b060	4350	1.72	−0.42	1.5	0.55	0.25	0.15	0.31	0.14	0.14	0.43
102180c6	b6b061	4550	1.86	−0.39	1.4	0.30	0.18	0.32	0.26	0.23	0.15	0.38
211484c6	b6b062	4800	1.92	−0.60	1.4	0.60	0.33	0.17	0.31	0.24	0.35	0.48
106969c6	b6b064	4950	1.98	−1.00	1.5	0.00	—	—	0.30	0.33	0.33	0.52
91438c6	b6b065	5150	2.10	−0.62	1.4	0.00	—	0.15	0.33	0.30	0.37	0.10
74262c6	b6b066	4950	2.08	−0.32	1.2	0.50	—	0.28	0.29	0.22	0.33	0.30
79869c6	b6b067	5300	2.23	−0.48	1.4	0.00	0.13	0.15	0.22	0.24	0.29	0.50
98974c6	b6b069	5200	2.12	−0.39	1.3	0.30	—	0.15	0.22	0.08	0.24	0.43
99069c6	b6b070	5400	2.27	−0.26	1.6	0.30	—	0.00	0.14	0.08	0.14	0.24
100384c6	b6b072	4550	1.83	−0.57	1.6	0.60	0.25	0.27	0.45	0.10	0.30	0.40
108928c6	b6b073	4850	1.96	−0.88	1.5	0.30	0.65	0.40	0.28	0.35	0.36	0.42
101274c6	b6b074	5150	2.14	−0.06	1.5	0.40	−0.10	—	0.14	0.00	0.20	0.48
71769c6	b6b075	5300	2.13	−0.22	1.5	0.60	0.20	0.08	0.22	0.11	0.23	0.23
62520c6	b6b077	4950	2.09	−0.84	1.5	0.50	0.30	0.10	0.25	0.30	0.25	0.32
60577c6	b6b078	4900	1.97	−0.18	1.5	0.10	0.10	—	0.30	−0.05	0.18	0.44
43679c6	b6b079	4950	2.10	−0.59	1.4	—	—	0.25	0.28	0.20	0.23	0.44
55804c6	b6b080	4100	1.54	0.19	1.5	0.00	−0.30	0.05	—	—	—	—
54561c6	b6b081	4900	1.97	−0.25	1.4	0.30	0.13	0.07	0.27	0.23	0.29	0.37
80281c6	b6b082	5050	2.15	−0.08	1.5	0.30	0.03	0.02	0.16	0.03	0.24	0.34
68782c6	b6b083	4750	1.93	−0.50	1.5	0.50	0.30	0.18	—	—	—	—
66376c6	b6b084	4650	1.87	0.19	1.5	0.30	−0.35	0.10	0.28	0.04	0.26	0.17
205837c7	b6b085	4750	1.95	−0.36	1.6	0.40	0.30	0.14	0.38	0.23	0.28	0.54
75097c7	b6b087	4550	1.82	−0.09	1.5	0.25	−0.10	0.07	0.16	−0.02	0.06	0.36
63747c7	b6b088	4950	2.02	−0.09	1.5	0.40	−0.07	0.10	0.23	0.15	0.10	0.39
46642c7	b6b090	4650	1.91	0.21	1.5	0.30	−0.28	−0.15	0.06	−0.06	0.07	0.14
57883c7	b6b091	4550	1.81	−0.25	1.5	0.40	0.15	0.13	0.23	0.13	0.33	0.38
51688c6	b6b092	4700	1.95	−0.42	1.5	0.40	0.27	0.12	0.37	0.19	0.33	0.59
209695c7	b6b093	4900	2.07	−0.11	1.4	0.40	0.03	−0.05	0.39	0.16	0.14	0.49
90337c7*	b6b095*	4700	1.70	−0.51	1.5	0.20	0.20	0.03	0.20	0.07	0.33	0.30
90337c7	b6b095	4850	2.02	−0.51	1.5	0.50	0.18	0.08	0.20	0.07	0.33	0.30
87232c7	b6b099	4950	2.03	−0.21	1.5	0.50	0.18	0.05	0.29	0.09	0.21	0.42
54480c7	b6b100	5100	2.08	−0.40	1.5	0.50	<0.00:	0.17	0.36	0.11	0.31	0.40
64860c7	b6b102	4500	1.80	0.09	1.5	0.55	−0.13	−0.27	0.18	−0.07	0.08	0.19
79003c7	b6b103	5200	2.08	−0.40	1.5	0.00	—	0.10	0.20	0.17	0.22	0.46
50439c7	b6b104	5100	2.16	−0.08	1.4	0.30	−0.20	0.10	0.34	−0.01	0.28	0.46
80144c7	b6b105	4750	1.83	−0.05	1.5	0.40	0.00	—	0.22	−0.01	0.10	0.14
97618c7	b6b107	4900	1.88	−0.91	1.5	—	—	0.30	0.21	0.41	0.20	0.47
102010c7	b6b108	4750	1.90	−0.56	1.4	0.40	0.25	0.22	0.38	0.14	0.34	0.56
87242c8	b6b109	4300	1.67	0.00	1.5	0.55	−0.08	—	0.24	0.13	0.26	0.10
88768c7	b6b111	4400	1.72	−0.25	1.5	0.40	−0.05	0.07	0.27	0.15	0.20	0.50
86105c7	b6b112	4900	2.06	−0.14	1.4	0.35	0.13	0.12	0.25	−0.01	0.35	0.51
77209c7	b6b113	4800	1.98	−0.43	1.3	0.40	0.35	0.23	0.35	0.31	0.33	0.50
98458c7	b6b114	4300	1.68	−0.02	1.5	0.60	0.00	0.00	0.26	0.30	0.06	0.07
5685c3	b6b116	4900	1.98	−1.15	1.5	0.00	—	0.28	0.20	0.44	0.20	0.50
104943c6	b6b117	5300	2.10	−1.20	1.5	—	—	0.40	—	—	—	—
5118c4	b6b118	4750	1.95	0.06	1.6	0.30	−0.08	0.03	0.16	−0.05	0.05	0.25
110465c7	b6b119	4600	1.90	0.00	1.4	0.30	−0.02	0.00	0.20	0.02	0.01	0.33
212654c8	b6b120	4850	2.01	0.39	1.4	0.10	−0.35	0.15	0.04	−0.10	0.25	0.02
108191c7	b6b121	5050	2.11	−0.77	1.5	0.00	—	—	0.32	0.30	0.35	0.55
23017c3*	b6b122*	4200	1.60	−0.01	1.5	0.20	0.03	−0.45	0.15	0.01	−0.02	0.17
23017c3	b6b122	4250	1.65	−0.01	1.5	0.35	0.07	0.00	0.15	0.01	−0.02	0.17
101167c8	b6b123	5100	2.16	0.05	1.5	0.65	0.45	−0.20	0.22	−0.02	0.16	0.30
103539c7	b6b124	4850	1.99	−0.31	1.5	0.50	—	0.14	—	—	—	—
202633c3	b6b126	4500	1.73	0.31	1.5	0.30	−0.30	—	0.14	0.05	0.01	0.11
32080c3	b6b127	5000	1.99	−0.17	1.6	0.50	0.10	0.05	0.28	0.06	0.06	0.39
43791c3	b6b128	4950	2.20	0.00	1.3	0.20	−0.15	0.03	0.07	0.04	0.06	0.18
204664c4	b6b129	5400	2.22	0.18	1.5	0.00	−0.30	−0.50	—	—	—	—
11653c3*	b6b132*	4900	1.80	0.04	1.6	0.30	−0.20	−0.45	0.18	−0.14	0.38	0.41

Table B.1. continued.

OGLE	GIRAFFE	T_{eff}	log g	[Fe/H]	v_t	[N/Fe]	[O/Fe]	[Zn/Fe]	[Mg/Fe]	[Si/Fe]	[Ca/Fe]	[Ti/Fe]
Field at −6° faint: B6-f												
11653c3	b6b132	4850	1.91	0.04	1.5	0.35	−0.30	−0.50	0.18	−0.14	0.38	0.41
21259c2*	b6b134*	4800	1.90	−0.29	1.3	0.30	0.15	0.05	0.29	−0.10	0.25	0.54
21259c2	b6b134	5000	2.02	−0.29	1.5	0.30	0.05	0.13	0.29	−0.10	0.25	0.54
200810c3	b6f003	4100	1.66	0.11	1.5	0.45	−0.20	−0.40	—	—	—	—
34058c3	b6f005	4400	1.84	0.21	1.6	0.50	−0.15	−0.10	0.13	0.02	0.00	0.09
47752c3	b6f006	3900	1.47	0.20	1.5	0.10	−0.30	0.00	—	—	—	—
40528c3	b6f008	4450	1.88	−0.48	1.7	0.10	0.10	0.22	0.39	0.30	0.08	0.40
29280c3*	b6f010*	4400	1.80	0.07	1.6	0.50	0.00	−0.25	0.08	0.00	0.01	0.00
29280c3	b6f010	4350	1.80	0.07	1.5	0.50	0.04	—	0.08	0.00	0.01	0.00
12982c3	b6f011	4300	1.95	0.01	1.5	0.70	−0.10	—	0.09	0.11	0.10	0.35
108051c7*	b6f013*	4100	1.60	0.03	1.3	0.10	−0.03	−0.15	0.24	0.13	0.15	0.36
108051c7	b6f013	4250	1.79	0.03	1.6	0.30	0.00	−0.05	0.24	0.13	0.15	0.36
20863c2	b6f015	4200	1.75	0.08	1.5	1.10	—	—	0.20	0.02	0.12	0.09
31220c2*	b6f016*	4700	2.00	0.10	1.6	0.50	−0.12	−0.44	0.20	0.20	−0.07	0.03
31220c2	b6f016	4400	1.81	0.10	1.7	0.40	−0.15	−0.05	0.20	0.20	−0.07	0.03
50086c2	b6f017	4350	1.80	0.32	1.5	0.30	−0.30	−0.30	0.08	−0.04	0.18	0.11
208608c3	b6f018	4750	2.06	−0.56	1.5	0.40	—	0.25	0.25	0.28	0.16	0.38
58159c3	b6f020	4400	1.93	−0.09	1.5	0.30	−0.02	0.00	0.15	0.06	0.10	0.23
70770c3	b6f021	4050	1.61	−0.04	1.5	0.40	0.00	0.00	—	—	—	—
205096c2	b6f023	4800	2.10	−0.15	1.4	0.40	0.00	0.02	0.14	0.07	0.12	0.07
148090c2	b6f024	4700	2.05	−0.28	1.5	0.30	—	—	—	—	—	—
42348c2	b6f025	4400	1.84	−0.09	1.5	0.30	—	−0.15	0.19	0.10	0.09	0.07
149531c2	b6f027	4500	1.91	−0.38	1.5	0.40	0.25	0.15	0.20	0.24	0.03	0.09
31090c2*	b6f028*	4600	1.90	−0.37	1.8	0.30	0.15	−0.08	0.35	0.09	0.12	0.39
31090c2	b6f028	4700	1.98	−0.37	1.5	0.10	0.05	0.14	0.35	0.09	0.12	0.39
14261c2	b6f029	4200	1.72	0.40	1.4	0.00	−0.30	0.00	—	—	—	—
69986c2	b6f030	4650	2.01	−0.27	1.5	0.35	0.13	0.05	0.38	0.14	0.19	0.53
73344c2	b6f031	4500	2.05	0.00	1.5	0.40	−0.05	−0.15	—	—	—	—
139560c2	b6f034	4300	1.87	0.26	1.5	0.20	−0.30	—	0.05	−0.08	0.04	0.07
145595c2	b6f035	4300	1.81	0.44	1.5	−0.15	−0.30	−0.10	−0.06	−0.08	0.07	0.09
22905c2	b6f036	4500	1.89	−0.45	1.4	0.35	0.28	0.25	0.37	0.24	0.19	0.32
47298c2	b6f037	4350	1.79	−0.51	1.7	0.50	0.18	0.20	0.48	0.27	0.25	0.41
33601c1	b6f038	4400	1.94	0.29	1.6	0.20	−0.20	−0.20	−0.02	−0.16	0.07	0.03
43023c2	b6f039	4600	1.95	−0.46	1.4	0.40	—	—	0.30	0.20	0.32	0.30
107527c6	b6f042	3750	1.20	−0.96	1.5	0.40	—	—	—	—	—	—
31176c2	b6f043	4400	1.76	−0.22	1.5	0.50	0.05	0.05	0.29	0.06	0.19	0.29
17038c2	b6f044	4300	1.76	0.29	1.4	0.10	−0.35	−0.45	0.08	0.05	0.09	−0.13
103742c5	b6f045	4100	1.69	0.31	1.5	0.20	−0.30	—	—	—	—	—
959c2	b6f049	4650	2.00	−0.58	1.4	0.00	0.30	0.30	0.37	0.25	0.24	0.33
10584c2	b6f051	4500	1.91	−0.38	1.4	0.30	0.30	0.20	0.29	0.10	0.13	0.35
15094c1	b6f052	4600	2.01	−0.19	1.4	0.20	0.13	0.12	0.20	0.02	0.23	0.51
95371c6	b6f054	4500	1.92	−0.27	1.4	0.15	0.05	0.12	0.29	0.01	0.25	0.46
98734c6	b6f055	4700	1.99	−0.06	1.1	0.70	—	−0.20	—	—	—	—
103413c6	b6f056	4150	1.65	0.24	1.4	0.30	—	−0.20	0.11	0.13	0.08	−0.16
85625c5	b6f057	4250	1.82	0.15	1.5	0.40	−0.20	−0.15	0.08	0.03	0.09	0.05
91631c6	b6f058	4800	2.05	−0.28	1.5	0.45	0.13	0.03	0.32	0.26	0.21	0.49
95545c6	b6f059	4250	1.77	−0.45	1.3	0.55	0.40	0.30	0.44	0.42	0.25	0.42
96460c6	b6f061	4650	1.94	0.25	1.4	0.35	−0.25	−0.10	0.07	−0.06	0.21	0.17
83500c6*	b6f062*	4200	1.50	−0.01	1.4	0.35	0.00	−0.15	0.12	−0.06	0.08	0.46
83500c6	b6f062	4400	2.00	−0.01	1.4	0.60	−0.10	—	0.12	−0.06	0.08	0.46
72513c6	b6f064	4700	1.98	−0.48	1.7	0.35	0.28	0.15	0.34	0.12	0.20	0.39
69731c6	b6f065	4450	1.95	−0.19	1.5	0.20	—	—	0.28	0.07	0.19	0.39
73072c6	b6f066	4050	1.60	0.12	1.5	0.35	−0.25	−0.30	0.27	0.14	0.04	−0.10
56641c6	b6f068	4450	1.81	0.17	1.5	0.30	−0.25	−0.05	0.08	0.04	0.10	−0.04
Field at −6° faint: B6-f												
208907c6	b6f069	4900	2.09	−0.17	1.5	0.30	0.10	—	0.30	0.08	0.16	0.25
99166c6	b6f070	4300	1.81	0.04	1.4	0.60	−0.15	−0.10	0.24	0.16	0.29	0.26
71832c6	b6f071	4300	1.80	−0.09	1.4	0.60	0.04	0.10	0.20	0.18	0.14	0.19

Table B.1. continued.

OGLE	GIRAFFE	T_{eff}	log g	[Fe/H]	v_t	[N/Fe]	[O/Fe]	[Zn/Fe]	[Mg/Fe]	[Si/Fe]	[Ca/Fe]	[Ti/Fe]
77481c6	b6f072	4950	2.13	−0.28	1.5	0.50	0.10	0.08	0.33	0.19	0.19	0.46
91776c6	b6f073	4800	2.11	0.23	1.5	0.20	−0.30	−0.35	0.11	−0.09	0.14	0.15
93621c6	b6f074	4550	1.92	−0.22	1.5	0.50	0.12	0.05	0.21	0.19	0.29	0.38
99940c6	b6f075	4200	1.69	−0.25	1.6	0.50	0.00	0.05	0.33	0.24	0.08	0.16
53554c6	b6f078	4350	1.78	0.08	1.4	0.45	−0.15	−0.05	0.26	−0.02	0.23	0.26
63690c6	b6f079	4800	2.06	0.03	1.5	0.40	−0.20	−0.02	0.07	−0.10	0.12	0.37
205097c6	b6f080	4700	2.18	0.26	1.4	0.20	−0.20	−0.20	−0.04	−0.13	0.03	0.00
52922c6	b6f081	4500	1.94	−0.30	1.5	0.40	0.18	0.05	0.33	0.09	0.16	0.27
51954c6	b6f082	4300	1.76	0.03	1.5	0.20	−0.20	0.02	0.12	0.15	0.08	0.03
56533c6	b6f083	4300	1.72	0.13	1.5	0.50	−0.20	−0.20	0.16	0.14	0.03	−0.11
94909c7	b6f084	4250	1.73	−0.11	1.4	0.80	−0.10	−0.55	0.17	0.19	0.26	0.28
73484c7	b6f085	4600	2.07	0.31	1.2	0.15	−0.35	−0.40	−0.22	−0.17	0.30	0.55
90995c7	b6f086	4800	2.07	−0.03	1.4	0.40	—	—	0.21	−0.08	0.24	0.20
41505c7	b6f087	4800	2.06	−0.48	1.6	0.30	0.10	0.20	0.36	0.18	0.19	0.46
34034c7	b6f088	4350	1.87	0.04	1.5	0.65	−0.10	−0.05	0.16	0.10	0.29	0.37
205852c7	b6f089	4350	1.86	0.06	1.5	0.50	−0.20	—	0.22	0.03	0.08	0.22
64944c7	b6f090	4350	1.79	0.08	1.5	0.35	−0.25	−0.20	0.11	0.02	0.28	0.19
75601c7	b6f091	4400	1.79	−0.08	1.5	0.55	−0.05	—	0.18	0.18	0.22	0.20
60208c7*	b6f092*	4400	1.90	−0.41	1.7	0.15	0.30	0.00	0.27	0.25	−0.02	0.13
60208c7	b6f092	4400	1.83	−0.41	1.6	0.53	0.30	0.12	0.27	0.25	−0.02	0.13
46088c7	b6f093	4500	1.90	−0.20	1.4	0.40	0.10	0.05	0.20	0.05	0.26	0.35
77743c7*	b6f095*	4600	1.90	0.11	1.8	0.50	−0.10	−0.30	0.04	0.05	−0.10	−0.05
77743c7	b6f095	4350	1.78	0.11	1.5	0.60	—	−0.15	0.04	0.05	−0.10	−0.05
85832c7	b6f096	4250	1.77	0.01	1.5	0.40	−0.20	—	0.23	0.09	0.11	0.05
211927c7	b6f097	4850	2.06	−0.81	1.0	0.00	—	—	—	—	—	—
93881c7	b6f098	4400	1.83	0.03	1.5	0.40	−0.10	−0.08	0.14	0.00	0.29	0.19
82739c7	b6f099	4600	1.99	−0.45	1.5	0.20	0.23	0.10	0.35	0.10	0.09	0.43
88860c7	b6f100	4450	1.85	−0.06	1.5	0.35	−0.15	−0.20	0.22	0.01	0.31	0.33
62874c7	b6f101	4600	1.92	−0.48	1.5	0.40	0.40	0.10	0.36	0.19	0.19	0.31
73636c7	b6f102	4450	1.86	−0.22	1.5	0.35	0.05	0.10	0.29	0.17	0.17	0.27
56730c7	b6f103	4300	1.83	0.00	1.3	0.30	−0.20	0.15	0.29	0.10	0.22	0.27
48678c7	b6f104	4750	2.00	0.17	1.6	0.40	−0.30	−0.15	0.22	0.01	0.10	0.18
58592c7	b6f105	4550	1.95	0.17	1.6	0.35	−0.25	—	0.01	−0.20	0.17	0.27
77419c7	b6f106	4600	1.93	0.18	1.5	0.30	−0.25	−0.15	0.05	0.00	0.14	0.10
96001c8	b6f107	4550	1.89	0.21	1.5	0.30	−0.30	−0.35	0.15	0.06	0.13	0.15
97453c7	b6f108	4700	2.00	0.02	1.5	0.45	−0.15	0.00	0.03	0.10	0.07	0.23
105594c7	b6f109	4900	2.10	−0.25	1.6	0.20	0.10	0.10	0.27	0.23	0.18	0.32
80262c8	b6f110	4700	2.06	0.23	1.5	0.25	−0.25	0.00	0.11	−0.08	0.21	0.22
80419c8	b6f111	4400	1.81	0.18	1.5	0.45	−0.20	−0.20	0.07	0.29	0.08	0.04
98090c7	b6f112	4550	1.88	−0.05	1.6	0.30	—	−0.15	0.00	0.03	0.04	0.26
75382c8	b6f113	4450	1.88	0.20	1.5	0.05	−0.30	−0.10	0.07	0.01	0.04	0.15
94445c7	b6f114	4550	1.93	−0.29	1.5	0.40	0.15	0.05	0.35	0.08	0.30	0.39
97069c7	b6f115	4100	1.61	0.25	1.5	0.35	−0.25	−0.50	—	—	—	—
132843c3	b6f116	4650	2.00	−0.05	1.5	0.00	—	—	—	—	—	—
8683c4	b6f117	4250	1.69	0.02	1.4	0.35	−0.05	0.00	0.11	0.01	0.13	0.18
215027c7	b6f118	4100	1.68	0.20	1.5	0.30	−0.30	−0.20	0.29	0.23	0.05	0.03
213817c7	b6f119	4450	1.86	0.27	1.5	0.05	−0.40	−0.40	0.08	−0.04	0.09	0.17
110776c7	b6f120	4600	1.84	−0.85	1.5	0.15	0.35	0.32	0.32	0.38	0.26	0.27
111007c8	b6f121	4300	1.81	0.01	1.4	0.45	−0.10	−0.20	0.14	0.02	0.10	0.16
108627c7	b6f123	4600	2.03	0.02	1.4	0.45	—	—	0.19	−0.02	0.10	0.39
97461c8	b6f124	4700	1.97	0.31	1.5	0.50	−0.10	−0.10	0.03	−0.05	0.11	0.26
35429c3	b6f126	4400	2.01	0.30	1.5	0.00	−0.30	−0.45	—	—	—	—
19346c3	b6f128	4900	2.09	0.27	1.5	0.20	−0.25	−0.17	0.02	−0.09	0.08	0.03
41112c4	b6f129	4500	1.89	−0.31	1.5	0.60	—	0.00	0.36	0.14	0.24	0.35
9081c3	b6f130	4500	1.93	−0.25	1.5	0.40	0.00	−0.05	0.39	0.09	0.16	0.51
35643c4	b6f131	5050	2.17	0.22	1.6	0.30	−0.35	−0.28	0.15	−0.10	0.35	0.48
27350c4	b6f134	4850	2.08	−0.36	1.3	0.00	0.00	0.20	0.25	0.15	0.37	0.41
6693c3	b6f135	4650	2.01	−0.03	1.5	0.50	−0.10	—	0.19	0.03	0.23	0.33